MECHANICALLY EXFOLIATED SINGLE AND MULTILAYER GRAPHENE SHEETS AND GRAPHENE FIELD EFFECT TRANSISTOR

by

Selin Manukyan

B.S., Physics, Boğaziçi University, 2008

Submitted to the Institute for Graduate Studies in
Science and Engineering in partial fulfillment of
the requirements for the degree of
Master of Science

Graduate Program in Physics
Boğaziçi University

2009

ACKNOWLEDGEMENTS

This work has been constructed around ideas belonging to my thesis co-superviser, *Prof. Dr. Ahmet Oral*. Beside many other things, I am grateful that he accepted my collaboration in this research, part of which became my M.S. thesis.

I would also like to thank to *Prof. Dr. Levent Kurnaz* for his all kind of support during my undergraduate study. Without his faith in me I would not be able to be at this level.

I would like to thank to my *smarty* friend *Erol Ertan* for his clever advice and to my best friend *Cem Yolcu* for his technical, emotional and mental support.

I am grateful to *Assist. Prof. Hidayet Çetin* at Bozok University for teaching me how to produce and characterize graphene, to *Selda Sonuşen* for helping me to take the contacts and collect data from graphene FET, to *Nihan Özkan* for sharing her AFM knowledge, to *Hüsnü Aslan*, *Derya Gemici* and *Dr. Özhan Ünverdi* for sharing their UHV knowledge with me.

I would like to thank to *Assoc. Prof. Mustafa Çulha* and his group at Yeditepe University for letting us use the Raman Spectroscope to characterize single layer graphene and *Dr. Güler Çelik* at SANAEM for taking Raman Spectroscopy data of graphene FET.

Finally, I would like to thank The Scientific and Technological Research Council of Turkey (TÜBİTAK) whose financial support through the grant 107T720 made life easier throughout my M.S. study.

ABSTRACT

MECHANICALLY EXFOLIATED SINGLE AND MULTILAYER GRAPHENE SHEETS AND GRAPHENE FIELD EFFECT TRANSISTOR

Graphene is a single layer of graphite sheet; one atom thick sp^2-bonded carbon atoms organized on a plane. It has extremely interesting electrical properties, which offers various applications in a number of nanometer scale devices, potentially operating at high frequency ranges. Mechanically exfoliated single and multilayer graphene sheets are prepared on (100) oriented silicon wafers with 300 nm thermal oxide. These graphene layers are characterized by optical microscopy, Atomic Force Microscopy (AFM) and Raman Spectroscopy. A graphene field effect transistor is fabricated on a 35×9 μm graphene sheet by manually applying the drain and source contacts using silver paint and using the silicon substrate as backgate. In this thesis, the production methods, characterization methods and electrical properties of graphene are investigated.

ÖZET

MEKANİK SOYMA YÖNTEMİ İLE ÜRETİLMİŞ TEK VE ÇOK TABAKALI GRAFEN YAPRAKLARI VE GRAFEN TEMELLİ ALAN ETKİLİ TRANSİSTÖR

sp^2 bağı ile birbirlerine bağlı karbon atomlarının oluşturduğu tek atomik katmanlı tabakaya grafen denir. Grafenin sahip olduğu olağanüstü elektriksel özellikleri nanometre mertebesinde çok geniş bir frekans aralığında çalışan birçok aygıtın yapımı için elverişlidir. Mekanik soyma yöntemi ile üretilmiş tek ve çok katmanlı grafen tabakaları üzeri 300 nm termal oksit kaplı silisyum (100) alttaşı üzerine aktarılmış ve optik mikroskop, Atomik Kuvvet Mikroskobu (AKM) ve Raman Spektroskopisi ile karakterize edilmiştir. Boyutları 35×9 μm olan grafen tabakasından gümüş boya kullanılarak el ile akaç ve kaynak bağlantıları yapılarak grafen alan etkili transistör üretilmiştir. Bu tezde grafenin üretim ve karakterizasyon yöntemleri ile elektriksel özellikleri incelenmiştir.

TABLE OF CONTENTS

LIST OF FIGURES

LIST OF TABLES

LIST OF SYMBOLS/ABBREVIATIONS

A	Ampere
$\mathcal{C}$	Contrast
d_1, d_2	Thicknesses of materials
E	Energy
h	Planck constant
$\hbar$	Reduced Planck constant
I	Intensity
k, k_x, k_y	Effective momentum
k_B	Boltzmann constant
n	Landau filling factor
n_0, n_1, n_2, n_3	Refractive indices
r, r_1, r_2, r_3	Relative indices of refraction
v_f	Fermi velocity
V	Volt
λ	wavelength of the light
σ	Hall conductivity
Φ_1, Φ_2	phase shifts due to optical path
AFM	Atomic Force Microscope
CVD	Chemical Vapor Deposition
EFM	Electric Force Microscope
FET	Field Effect Transistor
MOSFET	Metal-Oxide-Semiconductor Field Effect Transistor
PMMA	Poly(methyl methacrylate)
QHE	Quantum Hall Effect
SEM	Scanning Electron Microscope
STM	Scanning Tunnelling Microscope

1. INTRODUCTION

Around 70 years ago Landau [1, 2] and Peierls [3, 4] discussed theoretically whether a strictly two dimensional crystal can exist or not. They concluded that, in standard harmonic approximation [5], thermal fluctuations should destroy long-range order, resulting in melting of a 2D lattice at any finite temperature. Furthermore, Mermin and Wagner proved that the magnetic long-range order can not exist in one dimensions and later extended their proof to crystal line order in 2D [6, 7]. Furthermore, numerous experiments on thin films have been in agreement with the theory, showing that below a certain thickness, typically dozens of atomic layers, the films become thermodynamically unstable (segregate into islands or decompose), unless they constitute an inherent part of a three-dimensional (3D) system (like lattice matched heteroepitaxy). Although the theory does not allow perfect crystals in 2D space, it does not forbid nearly perfect 2D crystals in 3D space. Indeed, a detailed analysis of the 2D crystal problem beyond the harmonic approximation has led to the conclusion that the interaction between bending and stretching long-wavelength phonons could in principle stabilize atomically thin membranes through their deformation in the third dimension [8]. In 2004, Andre Geim and his research group discovered that freely suspended graphene can exist in two dimensions without a substrate and exhibit random elastic deformations involving all three dimensions [9].

Graphene is a one-atom-thick planar sheet of sp^2-bonded carbon atoms that are densely packed in a honeycomb crystal lattice. Within sp^2 hybridization, carbon atoms are σ bonded in the plane and π bonded between the planes. The carbon-carbon bond length in graphene is approximately 0.142 nm and the van der Waals diameter of one carbon atom is 0.34 nm. Carbon is a versatile element which can form single, double and triple bonds, thousands of chemical compounds and has numerous elemental structures and allotropes. Graphene exhibits high crystal quality, very high tensile strength, ballistic transport on a submicron scale (even under ambient conditions) and its charge carriers accurately mimic massless Dirac fermions. Graphene's perpendicular p-orbitals lead to electron delocalization because there is no distinction between neighboring π

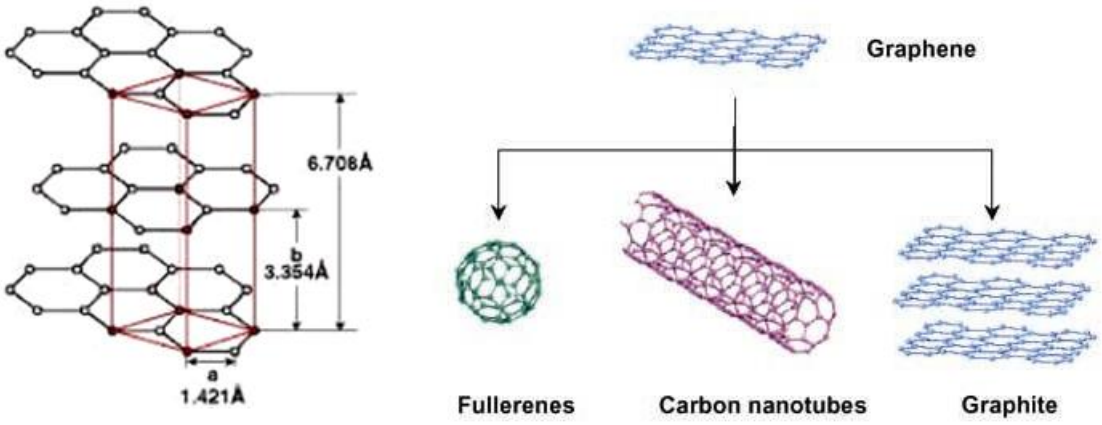

Figure 1.1. **a** is the carbon-carbon bond length in graphene and **b** is the van der Waals diameter.

bonds. This conjugated π orbital system permits the electrons to travel freely above and below the plane of carbon atoms with minimal scattering. This minimal scattering and strong delocalization properties makes graphene a good conductor.

1.1. PROPERTIES OF GRAPHENE

1.1.1. Electronic Properties

Intrinsic graphene is a semi-metal or zero-gap semiconductor. It was realized early on that the **E-k** relation is linear for low energies near the six corners of the two-dimensional hexagonal Brillouin zone, leading to zero effective mass for electrons and holes [35]. Due to this linear dispersion relation at low energies, electrons and holes near these six points, two of which are inequivalent, behave like relativistic particles described by the Dirac equation for spin $\frac{1}{2}$ particles. Hence, the electrons and holes are called Dirac fermions, and the six corners of the Brillouin zone are called the Dirac points. The equation describing the **E-k** relation is $E = \hbar v_f \sqrt{k_x^2 + k_y^2}$; where v_f, the Fermi velocity, is approximately 10^6 m/s.

The hexagonal structure of graphene has two characteristic electrical conduction paths as in Fig. 1.2. A very interesting characteristic of these two paths is that the zigzag path has metallic transport properties, while the armchair path is semiconduct-

ing [10].

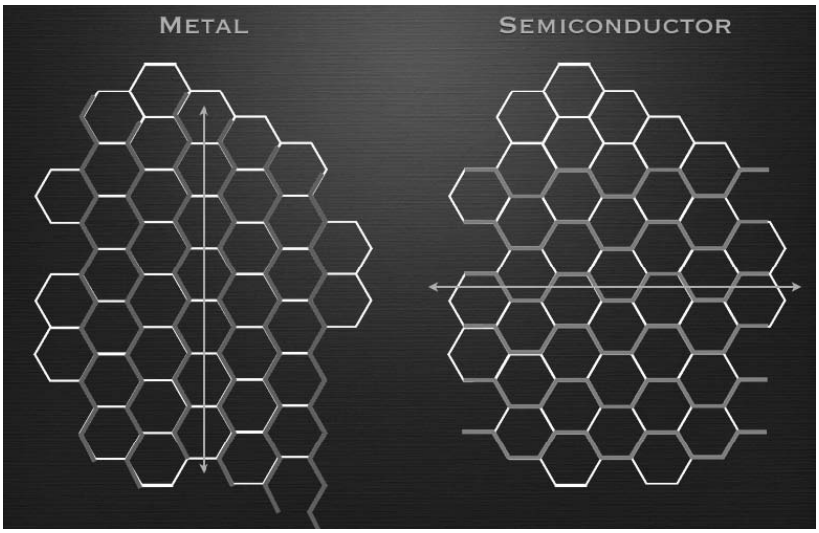

Figure 1.2. Zigzag (left) path shows with metallic transport and the armchair (right) path shows semiconducting transport properties. All other paths are a combination of the two, and due to their lack of symmetry, these paths are called chiral, since a reflection would describe a different path.

1.1.2. Electronic Transport

Experimental results from transport measurements show that the graphene has a remarkably high electron mobility at room temperature, with reported values in excess of 15,000 cm^2/Vs [11]. Additionally, the symmetry of the experimentally measured conductance indicates that the mobilities for holes and electrons are nearly the same. The mobility is nearly independent of temperature between 10 K and 100 K [12], which implies that the dominant scattering mechanism is defect scattering. Scattering by the acoustic phonons limits the intrinsic mobility of graphene to 200,000 cm^2/Vs at a carrier density of 10^{12} cm^{-2} at low temperatures. The corresponding resistivity of the graphene sheet would be $\sim 10^{-6}$ Ωcm, less than the resistivity of silver, the lowest resistivity material known at room temperature. However, for graphene on silicon dioxide substrates, scattering of electrons by optical phonons of the substrate is a larger effect at room temperature than scattering by graphenes own phonons, and this limits the mobility to $\sim$40,000 cm^2/Vs [13].

Despite the zero carrier density near the Dirac points, graphene exhibits a minimum conductivity on the order of $4e^2/h$. The origin of this minimum conductivity is still unclear. However, rippling of the graphene sheet or ionized impurities in the SiO_2 substrate may lead to local puddles of carriers that allow conduction. Several theories suggest that the minimum conductivity should be $4e^2/h\pi$. However, most measurements give $4e^2/h$ or slightly higher conductivity and depend on impurity concentration.

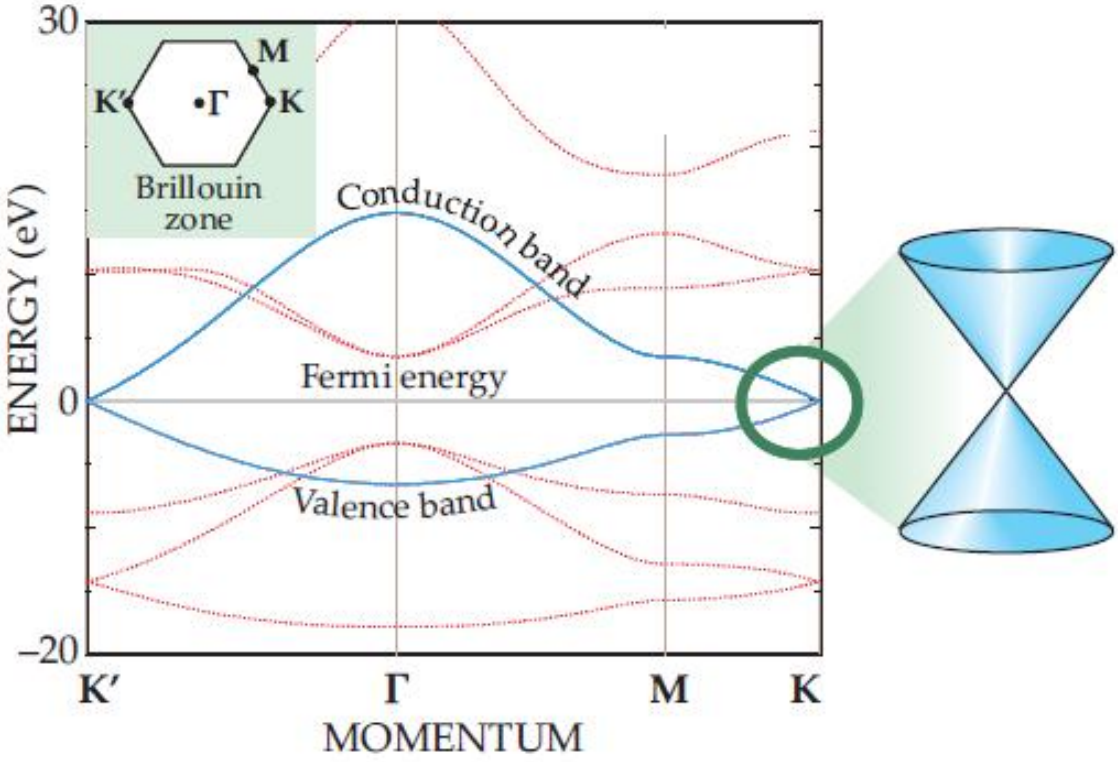

Figure 1.3. The Bloch band description of graphene. The π and π^* (blue) are decoupled from σ and σ^* bands (red) because of inversion symmetry [14]. The π bands have zero-gap energy.

Recent experiments have probed the influence of chemical dopants on the carrier mobility in graphene [15, 16]. Schedin *et al.* [16] doped graphene with various gaseous species (some acceptors, some donors), and found the initial undoped state of a graphene structure can be recovered by gently heating the graphene in vacuum. Schedin *et al.* reported that even for chemical dopant concentrations in excess of 10^{12} cm^{-2} there is no observable change in the carrier mobility. Chen *et al.* doped graphene with potassium in ultra high vacuum at low temperature. They found that potassium ions act as expected for charged impurities in graphene and can reduce the

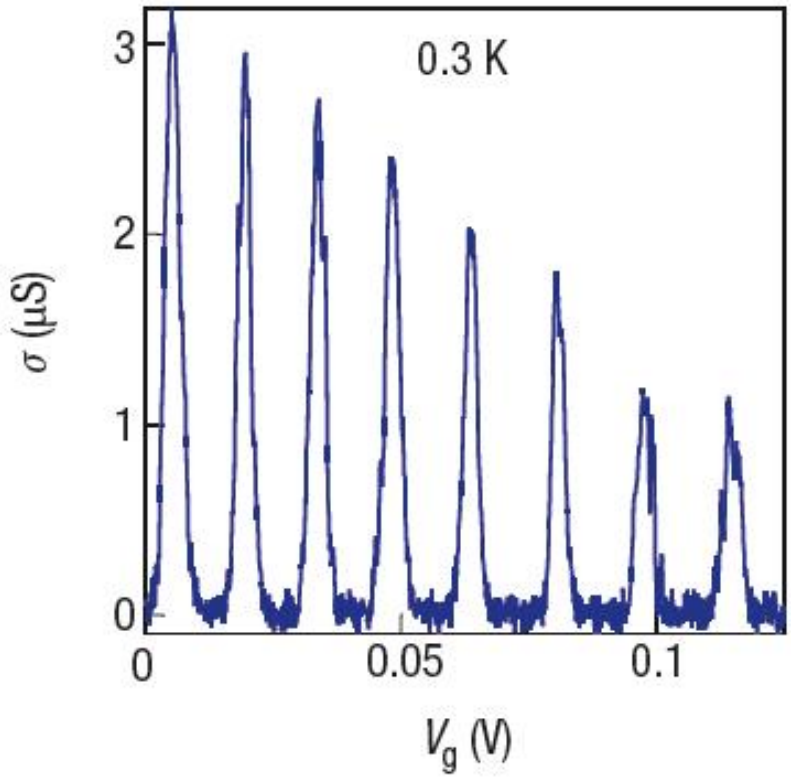

Figure 1.4. Coulomb blockade in relatively large quantum dots (diameter $\approx 0.25\mu$m) [14].

Table 1.1. Comparison of graphene with graphite.

	SINGLE LAYER GRAPHENE	GRAPHITE
Resistivity (Ω.cm)	10^{-6}	9×10^{-4} to 40×10^{-4}
Young Modulus (GPa)	500	9.2 to 12
Thermal Conductivity (W/mK)	~ 5×10^3	119 to 165
Carrier Density (cm^{-2})	10^{12}	10^3 to 10^9
Mobility (cm^2/V.s @ 300K)	15,000	~10,000
Mobility (cm^2/V.s@ 10K)	200,000	----------

mobility by a factor of 20 [15]. The mobility reduction is reversible on heating the graphene to remove the potassium.

1.1.3. Thermal Properties

The near-room temperature thermal conductivity of graphene was recently measured to be between $(4.84 \pm 0.44) \times 10^3$ to $(5.30 \pm 0.48) \times 10^3$ $\mathrm{Wm^{-1}K^{-1}}$ [17]. It can be shown by using the Wiedemann-Franz law, that the thermal conduction is phonon-dominated. It can be shown by using the Wiedemann-Franz law, that the thermal conduction is phonon-dominated. However, for a gated graphene strip, an applied gate bias causing a Fermi Energy shift much larger than $k_B T$ can cause the electronic contribution to increase and dominate over the phonon contribution at low temperatures.

In graphite, the c-axis (out of plane) thermal conductivity is over a factor of $\sim$100 smaller due to the weak binding forces between basal planes as well as the larger lattice spacing. In addition, the ballistic thermal conductance of a graphene is shown to give the lower limit of the ballistic thermal conductances, per unit circumference, length of carbon nanotubes [18].

Despite its 2-D nature, graphene has 3 acoustic phonon modes. The two in-plane modes have a linear dispersion relation, whereas the out of plane mode has a quadratic dispersion relation. Due to this, the T^2 dependent thermal conductivity contribution of the linear modes is dominant at low temperatures than the $\mathrm{T}^{1.5}$ contribution of the out of plane mode. The ballistic thermal conductance of graphene is isotropic [19, 20].

1.1.4. Mechanical Properties

The Young's modulus of graphene is 500 GPa, which differs from that of the bulk graphite. These high values make graphene very strong and rigid.

Table 1.2. Young's Modulus for various materials.

Young's Modulus For Various Materials	
Material	**GPa**
Aluminium	69
Diamond	1220
Silicon Carbide	450
Steel	200
Titanium	107
Graphene	500

1.1.5. Optical Properties

Graphene's unique electronic properties produce an unexpectedly high opacity for an atomic monolayer, with a startlingly simple value. It absorbs $\pi\alpha = 2.3\%$ of white light, where $\alpha = \frac{1}{137}$ is the fine-structure constant [21, 22]. Geim and his group observed graphene on 300 nm thick SiO_2 using optical microscope for the first time. Even though graphene is one atom thick, under certain conditions this single layer of carbon atom can be seen on optical microscope. Fresnel equations can be used to calculate the contrast seen on the optical microscope, which is widely used to find the mechanically exfoliated graphene flakes on substrates. The calculations are explained below.

In our case, we have a graphene-SiO_2-Si(100) sandwich as shown in Figure 1.5. We divided the problem into two parts to make the calculation easier. For the first part, the Fresnel coefficient of the SiO_2/Si(100) system is calculated.

$$r' = \frac{r_2 + r_3 e^{i\Phi_2}}{1 + r_2 r_3 e^{i\Phi_2}} \tag{1.1}$$

where

$$r_2 = \frac{n_1 - n_2}{n_1 + n_2},\ r_3 = \frac{n_2 - n_3}{n_2 + n_3}, \tag{1.2}$$

and n_1, n_2, n_3 are the refractive indices of graphene, SiO_2 and Si(100) respectively.

In the second part, the Fresnel coefficient of the air-graphene system is calculated.

$$r = \frac{r_1 + r_2 e^{i\Phi_1}}{1 + r_1 r_2 e^{i\Phi_1}} \tag{1.3}$$

where

$$r_1 = \frac{n_0 - n_1}{n_0 + n_1},\ r_2 = \frac{n_1 - n_2}{n_1 + n_2}, \tag{1.4}$$

and n_0 and n_1 are the refractive indices of air and graphene respectively. The final result can be found by combining of Equation 1.1 and Equation 1.3 .

$$r = \frac{r_1 + r' e^{i\Phi_1}}{1 + r_1 r' e^{i\Phi_1}} \tag{1.5}$$

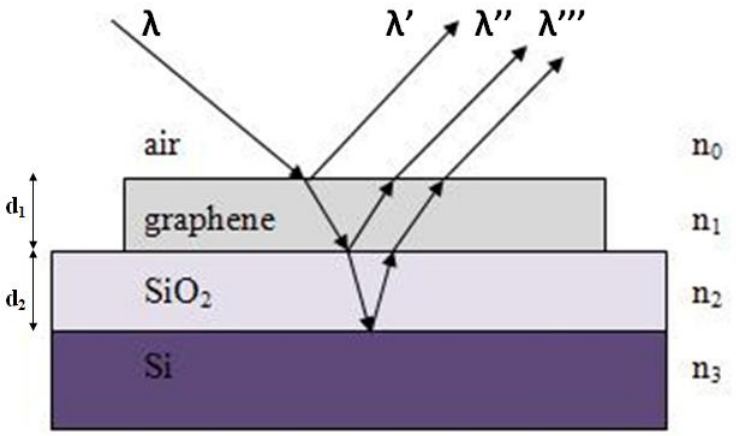

Figure 1.5. Reflection of light from a graphene sheet on the silicon substrate.

The intensity of reflected light can be found as

$$I(n_1) = \left| \frac{r_1 e^{i(\Phi_1+\Phi_2)} + r_2 e^{-i(\Phi_1-\Phi_2)} + r_3 e^{-i(\Phi_1+\Phi_2)} + r_1 r_2 r_3 e^{i(\Phi_1-\Phi_2)}}{e^{i(\Phi_1+\Phi_2)} + r_1 r_2 e^{-i(\Phi_1-\Phi_2)} + r_1 r_3 e^{-i(\Phi_1+\Phi_2)} + r_2 r_3 e^{i(\Phi_1-\Phi_2)}} \right|^2 . \tag{1.6}$$

where

$$r_1 = \frac{n_0 - n_1}{n_0 + n_1},\ r_2 = \frac{n_1 - n_2}{n_1 + n_2},\ r_3 = \frac{n_2 - n_3}{n_2 + n_3} \tag{1.7}$$

are the relative indices of refraction of air-graphene, graphene-SiO_2 and SiO_2-Si(100) systems respectively.

$$\Phi_1 = \frac{2\pi n_1 d_1}{\lambda} \qquad and \qquad \Phi_2 = \frac{2\pi n_2 d_2}{\lambda} \tag{1.8}$$

are the phase shifts due to changes in the optical path. The contrast $\mathcal{C}$ is defined as the relative intensity of reflected light in the presence ($n_1 \neq 1$) and absence ($n_1 = 1$) of graphene,

$$\mathcal{C} = \frac{I(n_1 \neq 1) - I(n_1)}{I(n_1 \neq 1)} \tag{1.9}$$

In Figure 1.6, optical contrast of single layer graphene deposited on SiO_2/Si(100) surface is plotted as a function of incident light wavelength and SiO_2 layer thickness. Figure 1.7 shows the detailed contrast dependence of SiO_2 thickness for 90, 200 and 300nm respectively, as a function of wavelength.

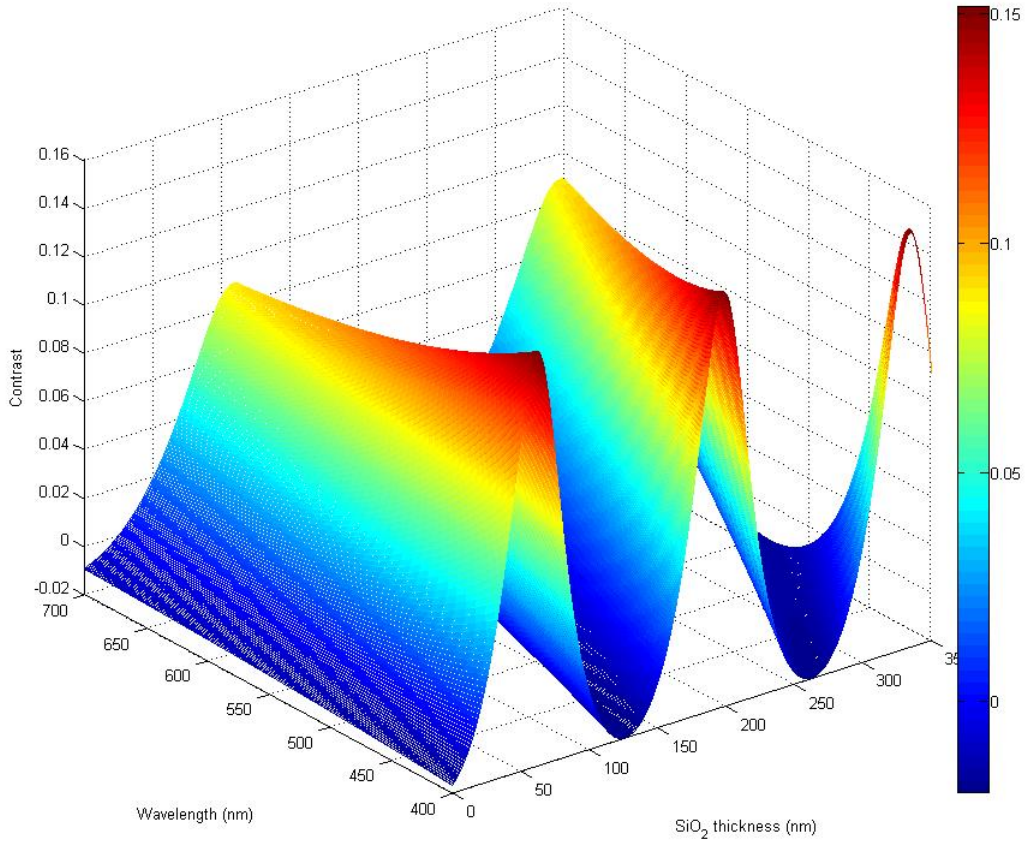

Figure 1.6. Contrast of graphene as a function of wavelength and SiO_2 thickness.

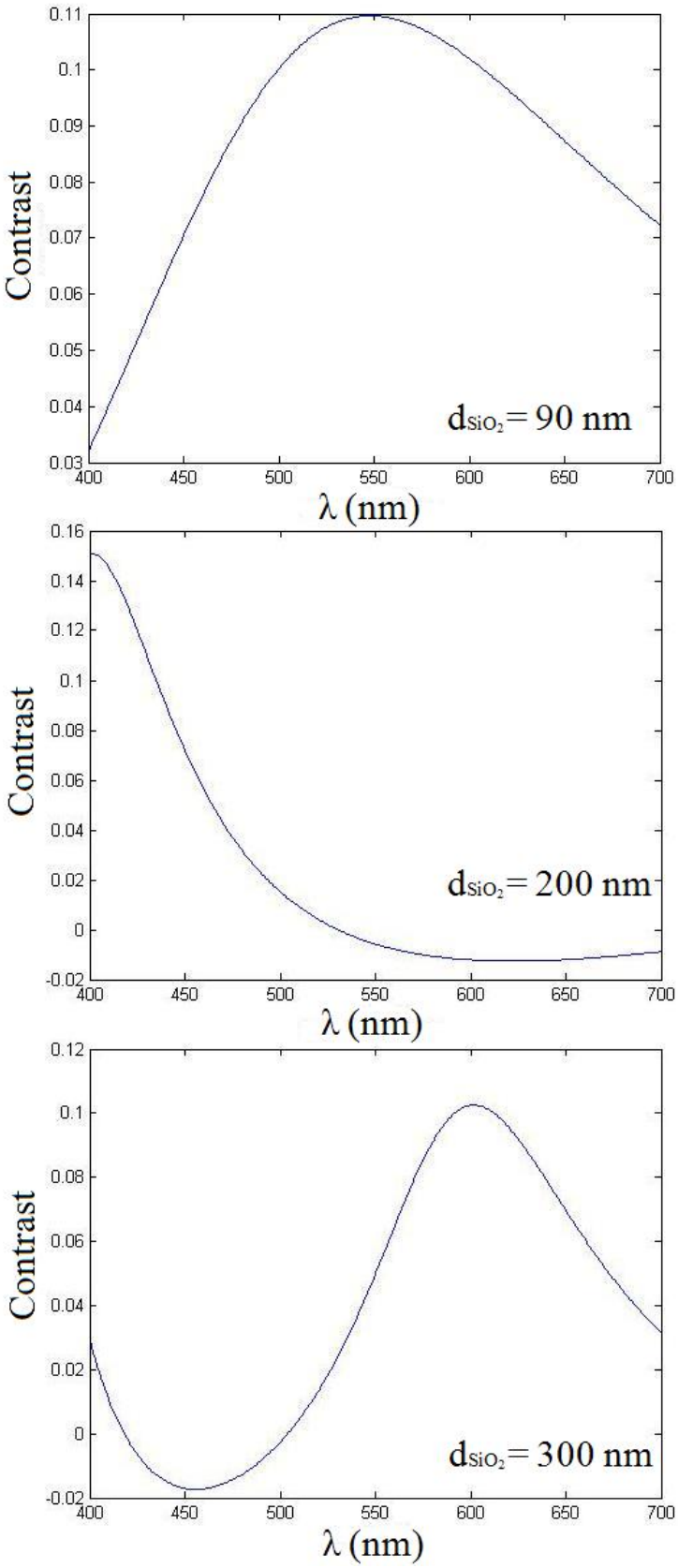

Figure 1.7. Contrast of single layer graphene as a function of wavelength λ for 90/200/300 nm SiO_2 thickness on Si(100) substrate.

1.1.6. Anomalous Quantum Hall effect

The integer quantum Hall effect is a quantum-mechanical version of the Hall effect, observed in two-dimensional electron systems subjected to strong magnetic fields, in which the Hall conductivity σ takes on the quantized values [23]

$$\sigma = n\frac{e^2}{h} \tag{1.10}$$

where n is the Landau filling factor (n=1,2,3,...), e is elementary charge and h is the Planck constant.

Graphene displays *anomalous* quantum Hall effect in the presence of a magnetic field, but these remarkable anomalies can even be measured at room temperature [12]. This anomalous behavior is a direct result of the massless Dirac electrons in graphene. In a magnetic field, their spectrum has a Landau level with energy precisely at the Dirac point. The quantized conductivity steps are shifted by $\frac{1}{2}$ with respect to the standard sequence and with an additional factor of 4 coming form the double valley and double spin degeneracies.

$$\sigma = \pm 4(n + 1/2)\frac{e^2}{h} \tag{1.11}$$

In Figure 1.8 the image (a) shows the values of transverse conductivity σ_{xy} at the surrounding plateaus imply that this level is drawn half from the conduction band and half from the valance band. The quantum Hall effect proves that charge carriers in single layer graphene are massless Dirac fermions. The image (b) shows the quantization at n=0 reveals that bilayer graphene is made up of massive, chiral fermions [14].

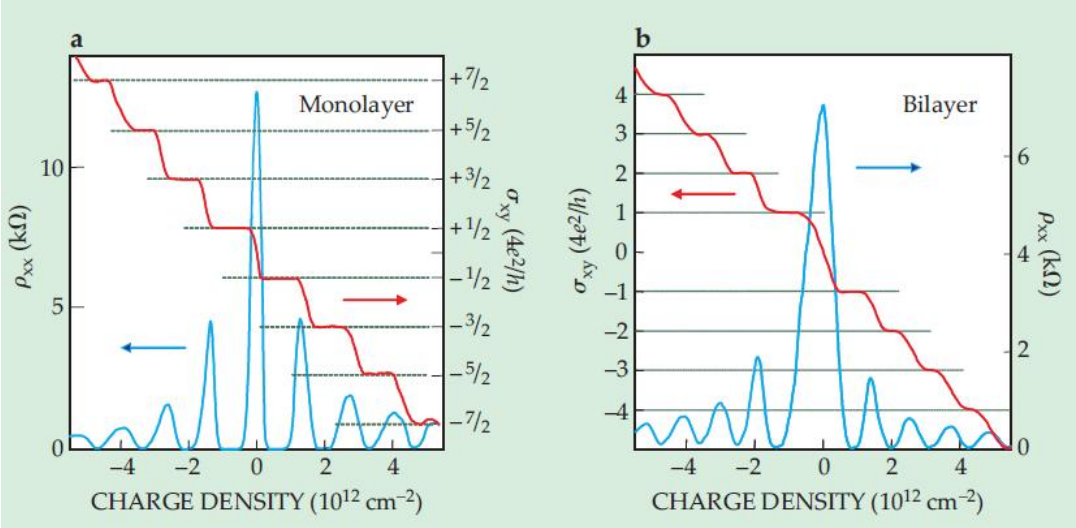

Figure 1.8. Quantum Hall Effect in graphene as a function of charge-carrier density n.

1.2. PRODUCTION METHODS OF GRAPHENE

1.2.1. Exfoliation Method

In this method 3D graphite crystals are peeled repeatedly with Scotch Magic ® or Pritt Invisible tape and transfered onto Si(100) wafer with 300 nm thermal oxide. We can prepare freely suspended graphene flakes on SiO_2 or other substrates like PMMA etc. with this method. The silicon substrate beneath the silicon dioxide is used as a "back gate" electrode to control the charge density in the graphene layer over a quite wide range.

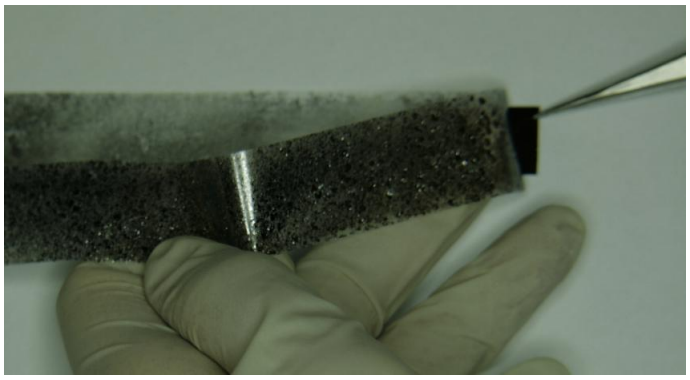

Figure 1.9. Transfer of graphene on SiO_2 layer.

1.2.2. Epitaxial Growth Of Graphene On Silicon Carbide, Ruthenium And Other Metals

Silicon Carbide (SiC), also known as carborundum, has Zinc Blend crystal structure. It occurs in nature as an extremely rare mineral moissanite. Production steps of graphene out of SiC consists of polishing and annealing the SiC(1000) wafer. First the SiC wafer is etched under H_2 environment at 1400-1600 °C. This procedure etches the surface and cleans the scratches formed during the polishing steps used for the wafer production, generating clean atomic terraces on the wafer. After etching, the sample is annealed at 1100-1500 °C under ultra high vacuum. During this process, silicon atoms evaporate faster than carbon atoms, leaving a carbon rich layer behind, which crystallizes into graphene layers epitaxially on SiC(1000)[24].

Epitaxial growth of graphene on ruthenium surface takes advantage of Ru (0001) atomic structure to seed the growth of the graphene [25]. During this chemical vapor deposition (CVD) procedure with ethylene gas, a very sparse graphene nucleation enables the growth of macroscopic single crystalline domains with dimensions exceeding 200 μm. The ability to control the CVD process parameters helps to determine the substrate interactions with graphene and consequently on the electronic properties of the epitaxial graphene. The first graphene layer adheres strongly to the ruthenium substrate, while the second layer is decoupled and acts like suspended graphene.

Graphene grown on ruthenium doesn't typically yield a sample with a uniform thickness of graphene layers and at high temperatures carbon is absorbed into the ruthenium bulk, which constructs a metalayer.

Significant differences between graphene epitaxy on Ru(0001) and SiC(1000) are obviously due to the process conditions. Si sublimation on SiC at high temperatures (between 1,250 and 1,450 °C) apparently leads to small (<1 μm) multilayer graphene to nucleate. Graphene epitaxy on Ru(0001) relatively at lower temperatures ∼850 °C produces sparse arrays of graphene nucleation that grows in a controlled layer-by-layer mode to macroscopic dimensions.

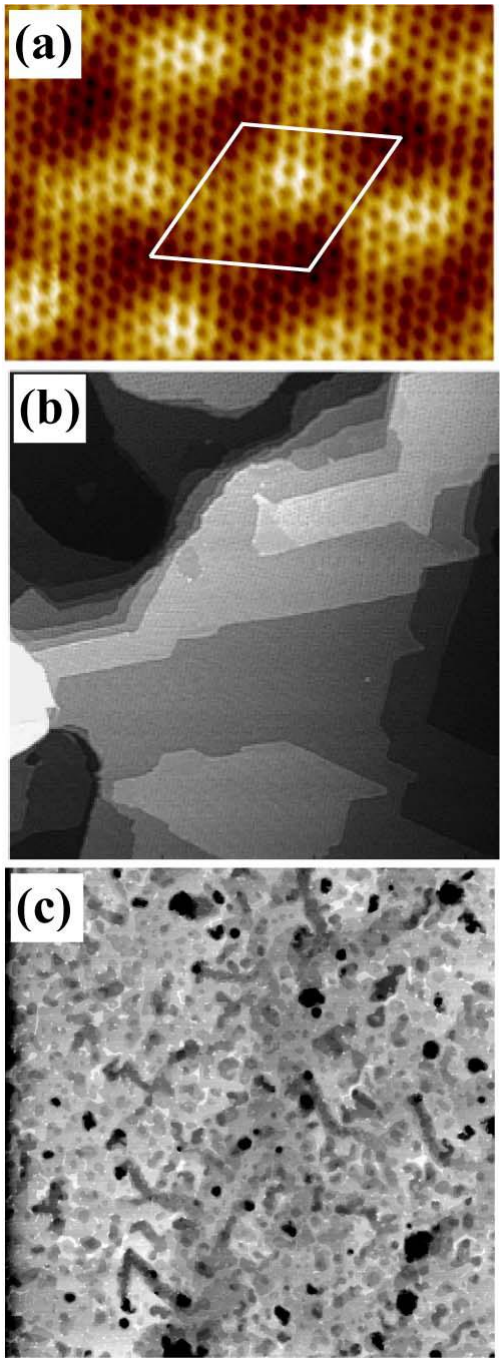

Figure 1.10. (a) STM image of Si-face graphene. (6x6) unit cell is shown for reference. (b) Large scale STM image. (c) Large scale AFM image [24].

High-quality sheets of few layer graphene exceeding 1cm^2 size have been synthesized via chemical vapor deposition (CVD) on thin nickel films. These sheets have been successfully transferred to various substrates, demonstrating viability for numerous electronic applications [26]. An improvement of this technique has been achieved on copper foil, where the growth automatically terminates after a single graphene layer, and arbitrarily large graphene films can be fabricated [27].

1.2.3. Chemical Methods

Beside physical methods, chemists are focused on producing gram-quantities of graphene by different methods. One of those methods is reducing the graphene oxide paper in a solution of pure hydrazine into graphene [28]. Another technique to produce graphene is the reduction of ethanol by sodium metal, followed by pyrolysis of the ethoxide product and washing with water to remove sodium salts. These methods aim the mass production of graphene, but in contrast to the epitaxial or mechanically exfoliated graphene, they have a large number of impurities and defects created during the process [29].

Dispersion and exfoliation of graphite in strong organic solvents such as N-methylpyrrolidone (NMP), N,N-Dimethylacetamide (DMA), γ-butyrolacetone (GBA) etc. are also an alternative method for mass production of graphene [30]. Sonication of graphitic flakes in these solutions creates graphene flakes and a centrifuge is used to segregate thin layers from thick flakes. Spray coating or drop casting of the buffer solution on silicon wafer coated with 300 nm thick thermal silicon oxide deposits the graphene flakes on the wafer. After evaporating the solution on the wafer, either in vacuum ovens or on hot plate, it is possible to observe graphene flakes on the wafer under optical microscope.

Graphene Production Methods	Mobility μ (cm^2/Vs)	Carrier Density n (cm^{-2})
Suspended Graphene at 240 K	120,000	$2x10^{11}$ (for electrons)
Suspended Graphene at 5 K	170,000-230,000	$0.5x10^{11}$-2 $x10^{11}$
Unsuspended Graphene at 300K	5,000-20,000	$7.2x10^{12}$
Unsuspended Graphene at 5K	60,000	---
CVD on polycrystalline Ni film	100-2,000	---
On PDMA (polydimethylsiloxane)	3,750	$5.0x10^{12}$
On 6H-SiC surface (3 layers)	1,110	$3.6x10^{12}$

Figure 1.11. The mobility and carrier density values of graphene for different production methods.

1.3. CHARACTERIZATION OF GRAPHENE

1.3.1. Optical Microscope

As mentioned in 1.1.5 graphene can be observed on 300 nm SiO_2 under white light where SiO_2 has a pinkish orange color. Before deposition of any graphene on the silicon wafer, the wafer should be cleaned properly. We use piranha solution which is a 3:1 mixture of 97% sulfuric acid (H_2SO_4) and 30 % hydrogen peroxide (H_2O_2) to remove the organic residues on the wafer. Then we exfoliate graphite pieces (flake graphite, flaggy flakes, flake size 3-10 mm, India origin, NGS Naturegraphit GmbH, Germany) with Scotch Magic ® Tape or Pritt Invisible tape until we see a very blur residue of graphite on the tape after repeatedly peeling of the band and transferring to the other tapes. After transferring the graphite residues on the wafer, we search for the graphene flakes under a ×50 objective lens attached to high quality optical microscope.

Single layer graphene has a very light greyish pink contrast on silicon wafer coated with 300 nm thick thermal silicon oxide. We used a Nikon Eclipse ME600 optical microscope with a Spot Insight QE camera.

In Figure 1.12 single, double and triple layers of graphene layers are clearly visible, which are on sale from Graphene Industries Limited for £500. Here the thickness of

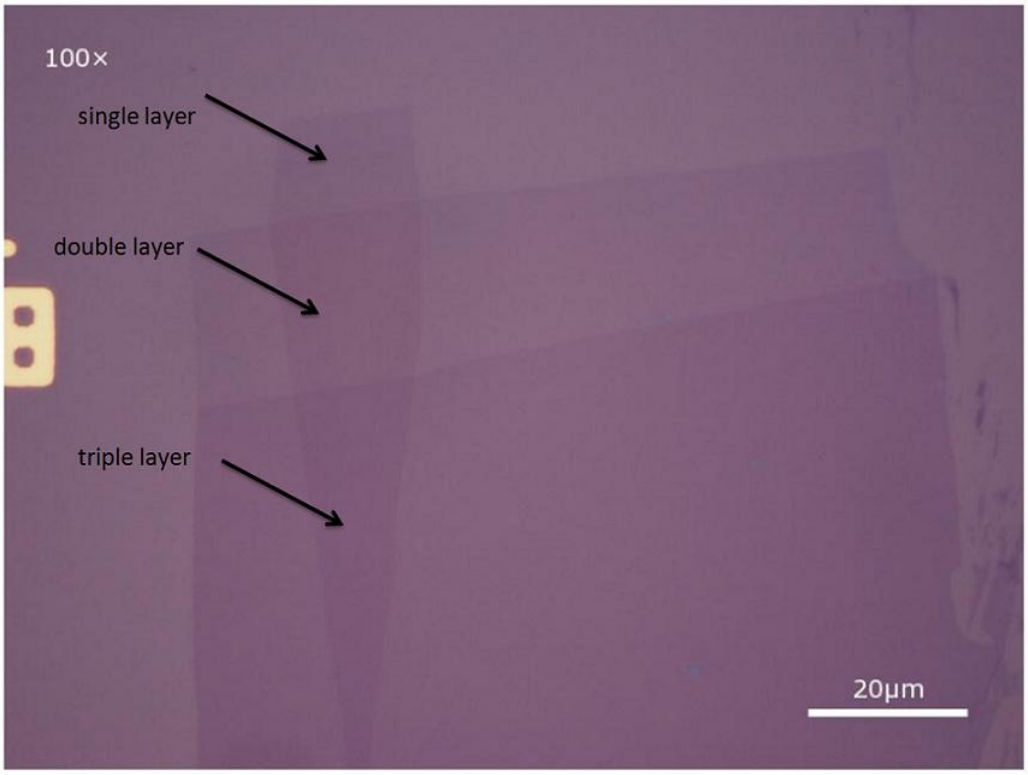

Figure 1.12. Optical microscope view of bilayer graphene sheets produced by *Graphene Industries Limited* [31].

the dry thermal oxide layer is 280-310 nm. These layers are produced by exfoliation method by using clean room tape instead of scotch tape, which breaks down under UV light and leaves minimum amount of adhesive residues. This company is established by Andre Geim's students at Manchester.

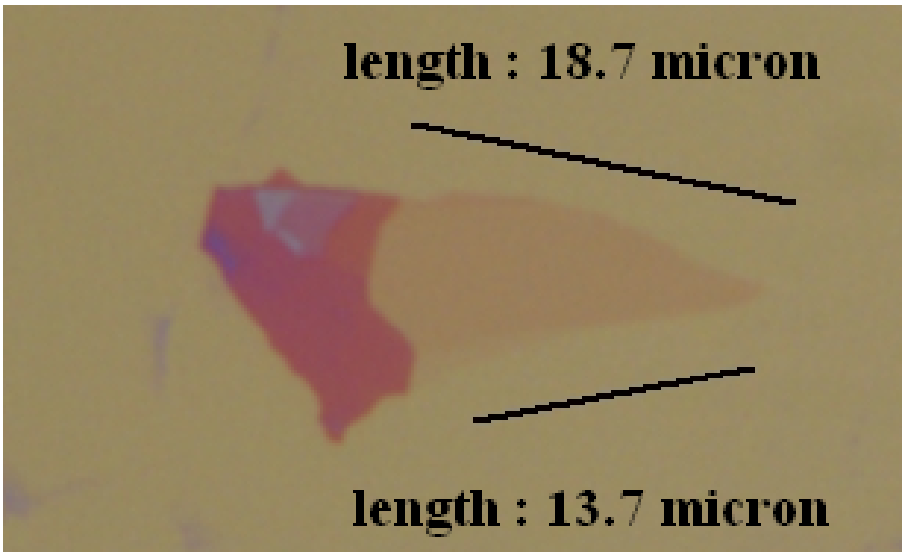

Figure 1.13. Optical microscope image of a three layer graphene produced by exfoliation method using flaggy flake graphite mesh size 3-10 microns (with ×50 objective lens).

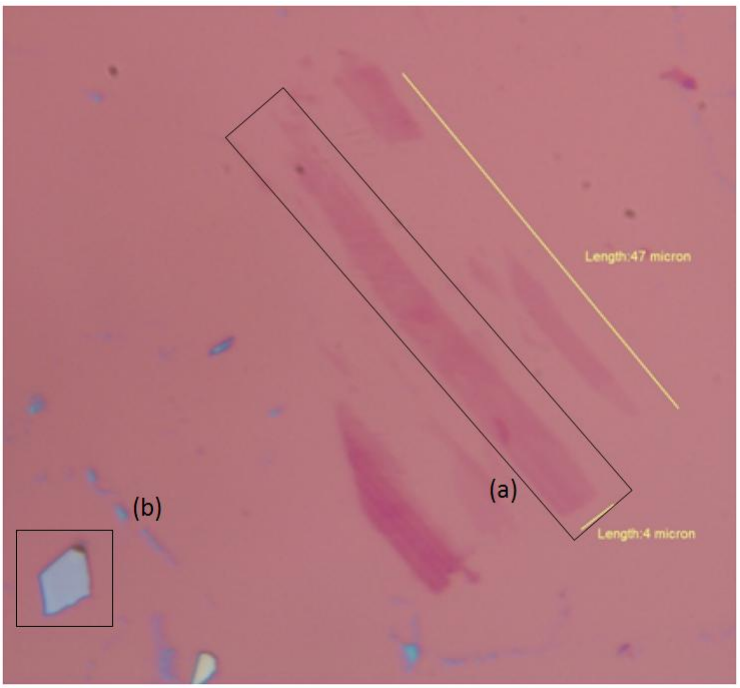

Figure 1.14. Optical microscope image of **(a)** single layer of graphene and **(b)** graphite piece produced by exfoliation method using flaggy flake graphite mesh size 3-10 microns (with ×50 objective lens).

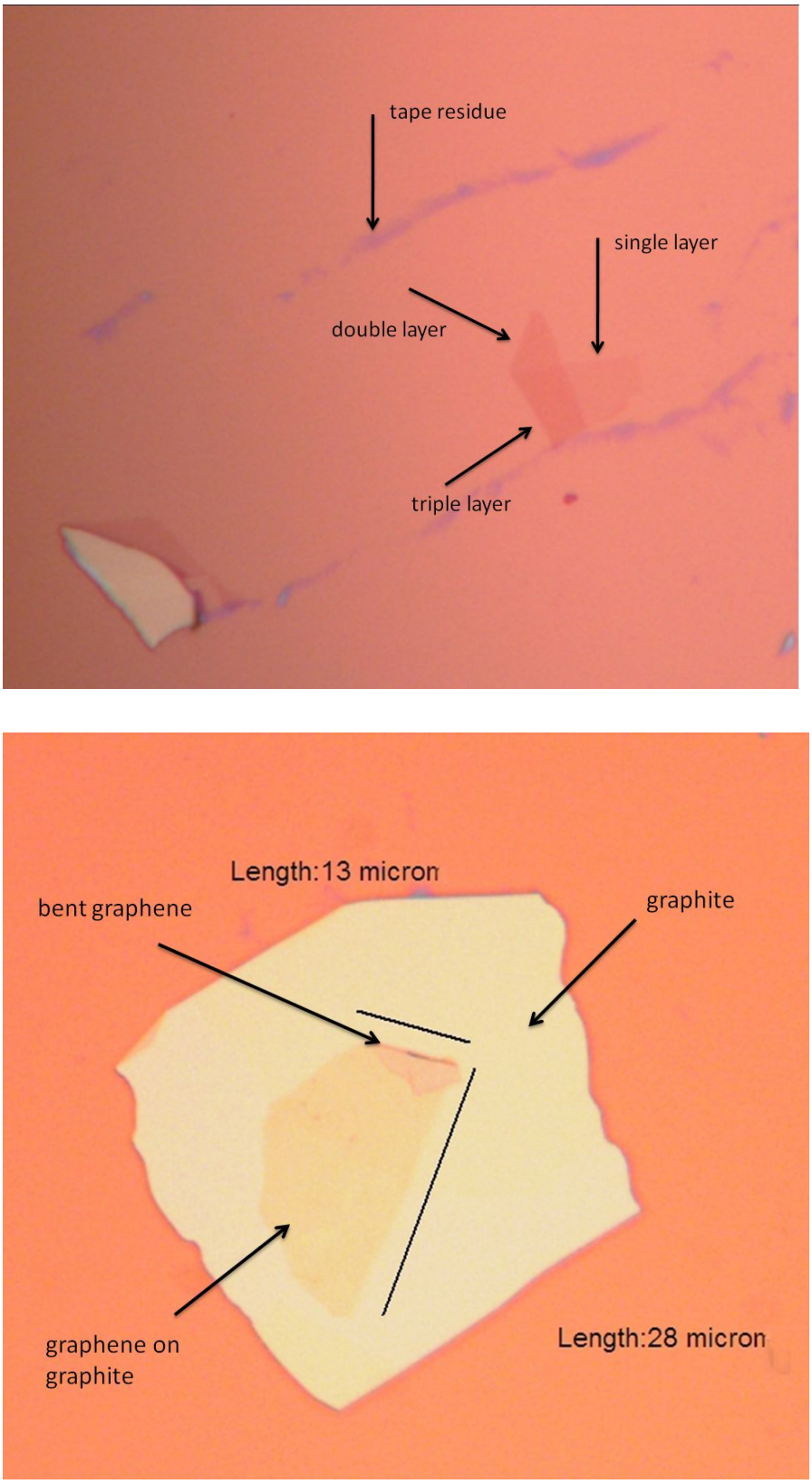

Figure 1.15. (top) Three different layers of graphene produced by exfoliation method using flaggy flake graphite mesh size 3-10 microns (with ×50 objective lens). (bottom) Suspended graphene sheet on graphite.

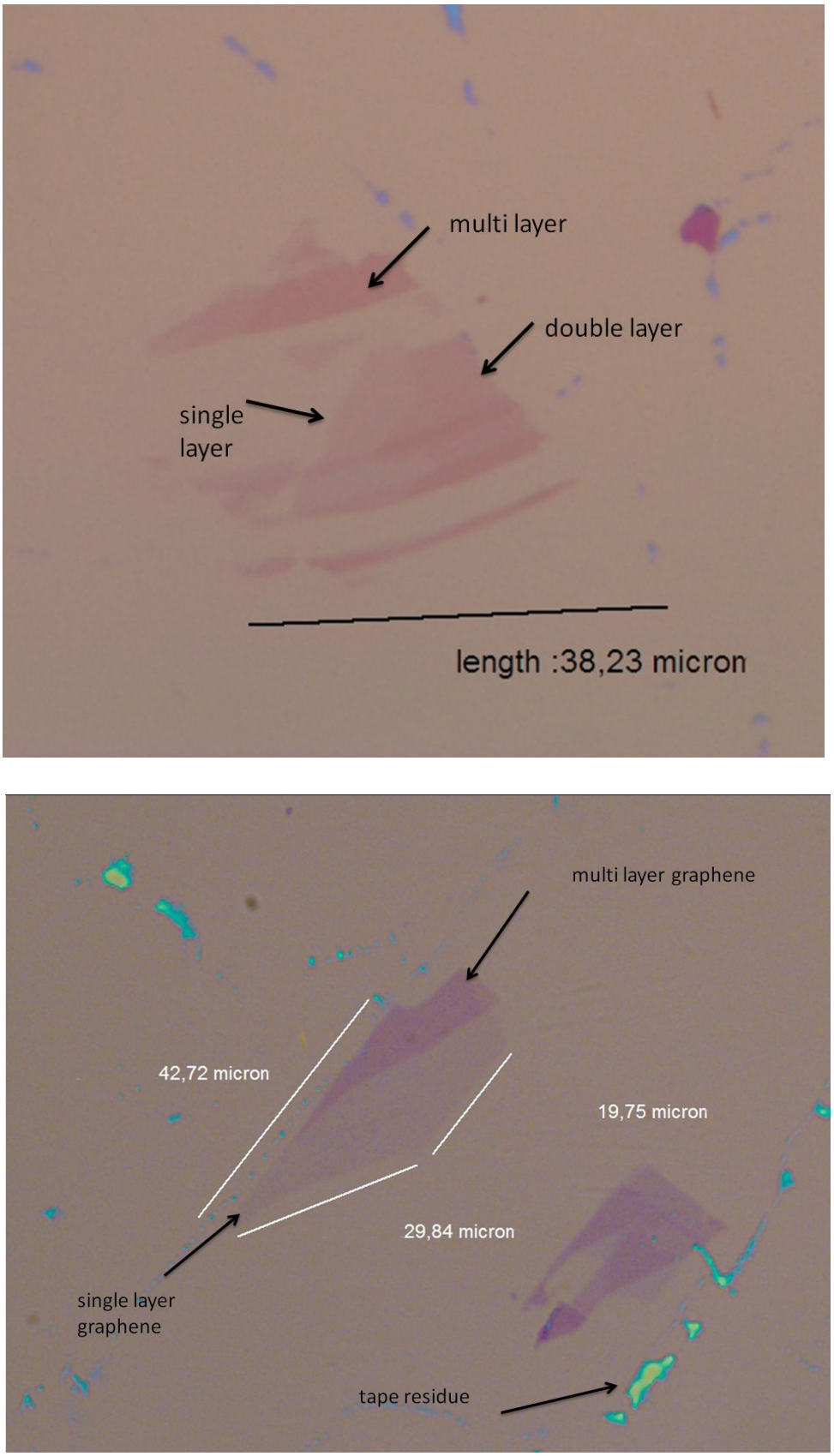

Figure 1.16. (top & bottom) Graphene produced by exfoliation method using flaggy flake graphite mesh size 3-10 microns (with ×50 objective lens).

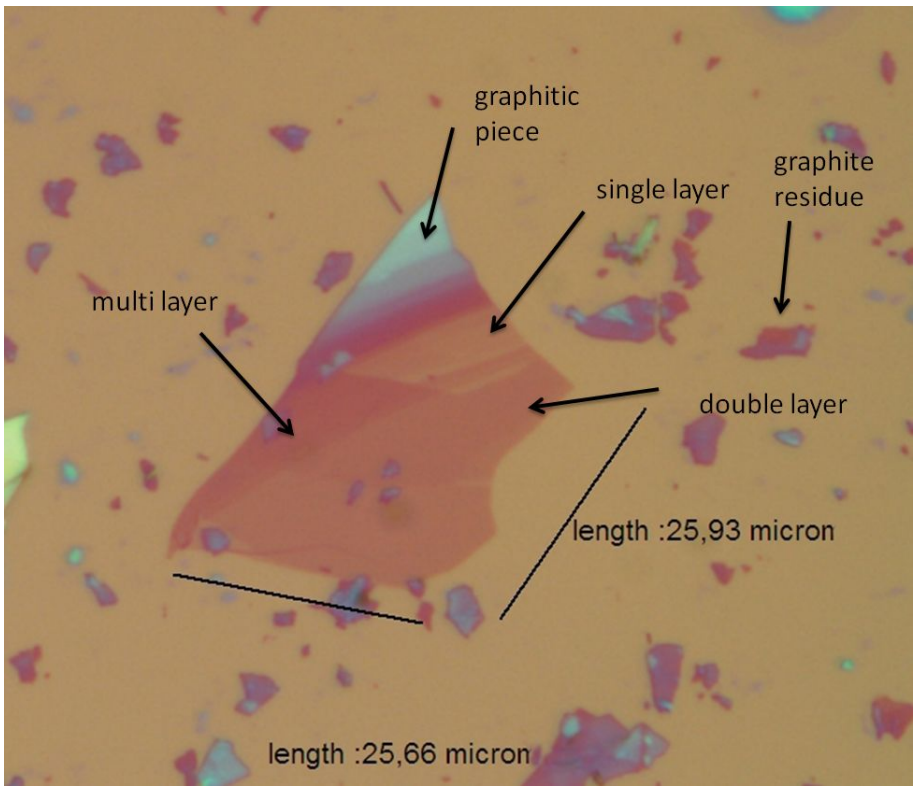

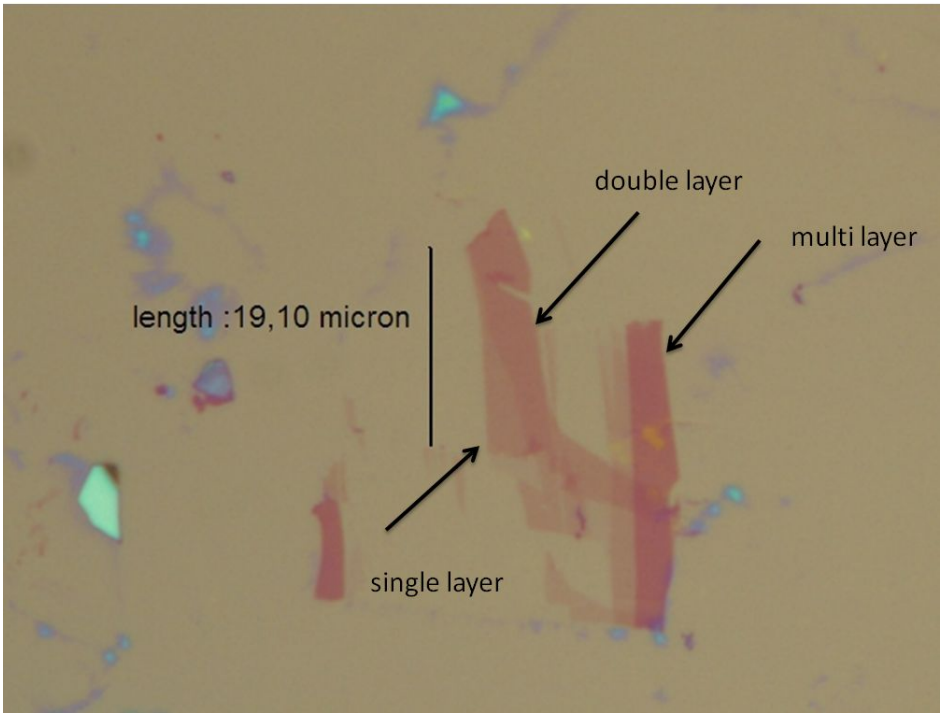

Figure 1.17. (top & bottom) Graphene produced by exfoliation method using flaggy flake graphite mesh size 3-10 microns (with ×50 objective lens).

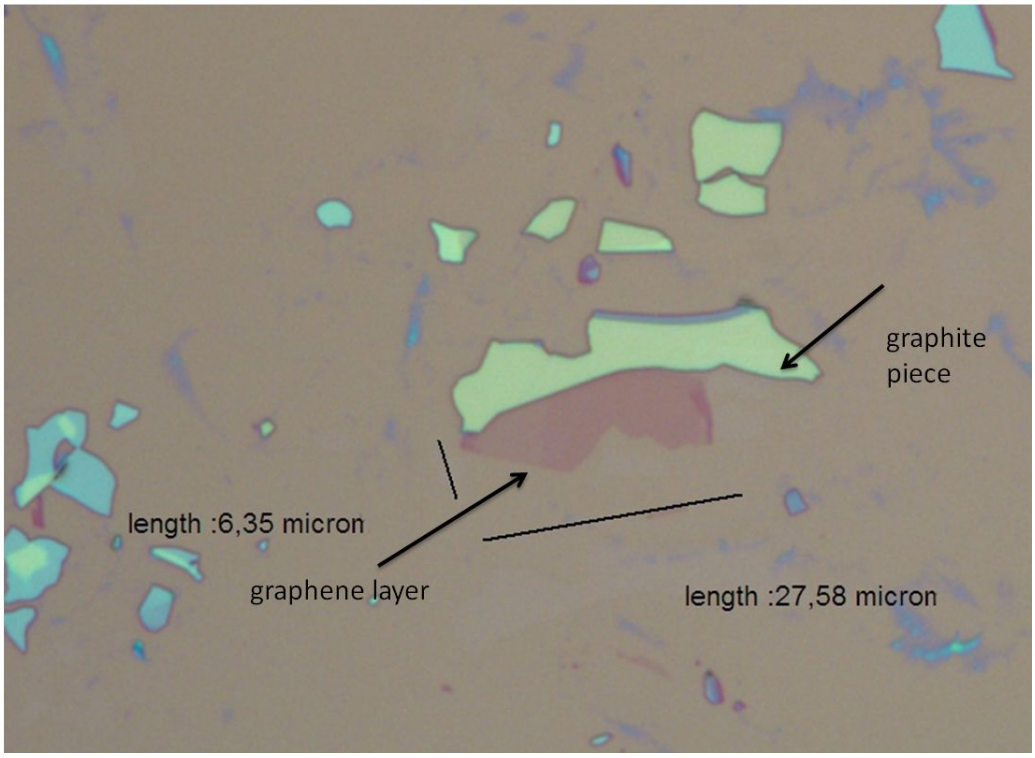

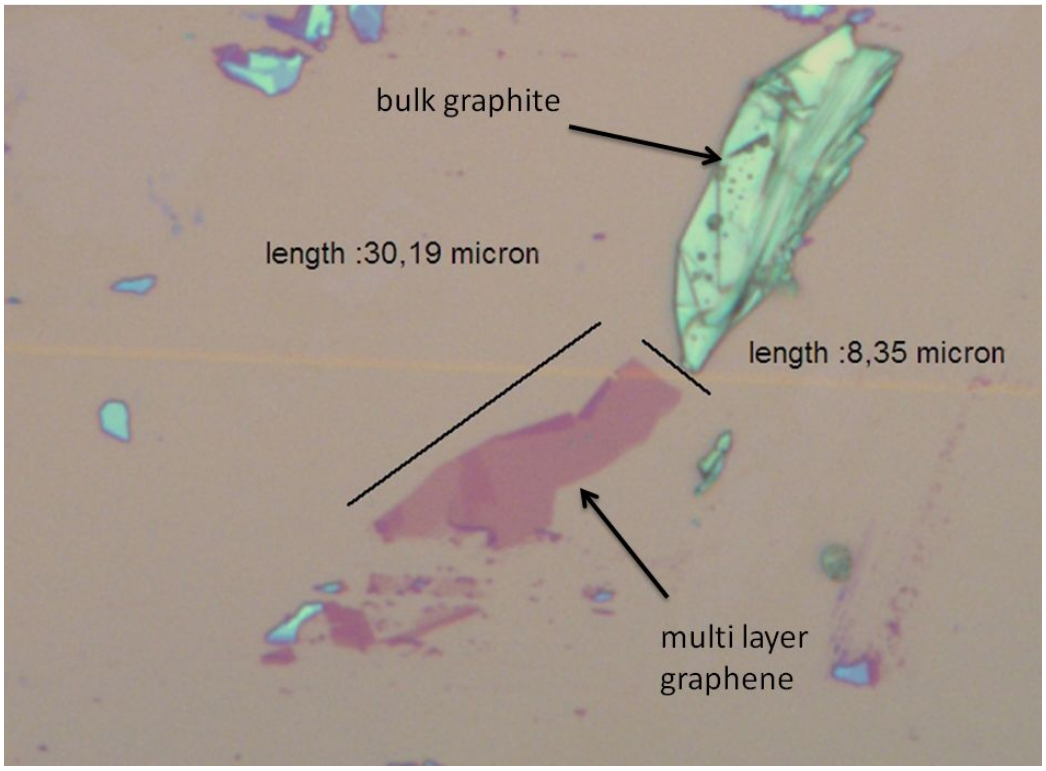

Figure 1.18. (top & bottom) Graphene produced by exfoliation method using flaggy flake graphite mesh size 3-10 microns (with ×50 objective lens).

1.3.2. AFM Characterization

We also imaged the graphene layers with an Atomic Force Microscope (AFM) supplied by NanoMagnetics Instruments Ltd. We operated the AFM in tapping mode. The cantilevers we used for this mode were single crystal silicon tips with 300 kHz resonant frequency and 40 N/m force constant. The typical scan speed was 1 μm/sec and the typical image size was 256×256 pixels. After determining the coordinates of the graphene on the substrate, we marked it with a permanent marker under optical microscope. Then we match the CCD camera view of marked graphene with the optical image and designate the scan area.

According to Moser *et al.* [32] the electric dipole of residues left from the adhesive tape during graphene preparation, as well as the dipole moments of water molecules adsorbed on top of graphene can be detected via EFM (Electric Force Microscope)(see Figure 1.21).

It is first observed that the water molecules and adhesive tape residues on pristine SiO_2 surface have a height of around 0.66 nm. After confirming the single layer graphene sheet via Raman Spectroscopy, it is scanned with EFM and observed a height of around 1 nm which also proved the height of water molecules accumulated on single layer graphene sheet ($\sim$0.34 nm single layer graphene + $\sim$0.66 nm water molecule residue $\cong$ 1 nm.). On the cross section image we observe a slope on the edge because of the cross coupling effect caused by the x-y motion of the scanner tube.

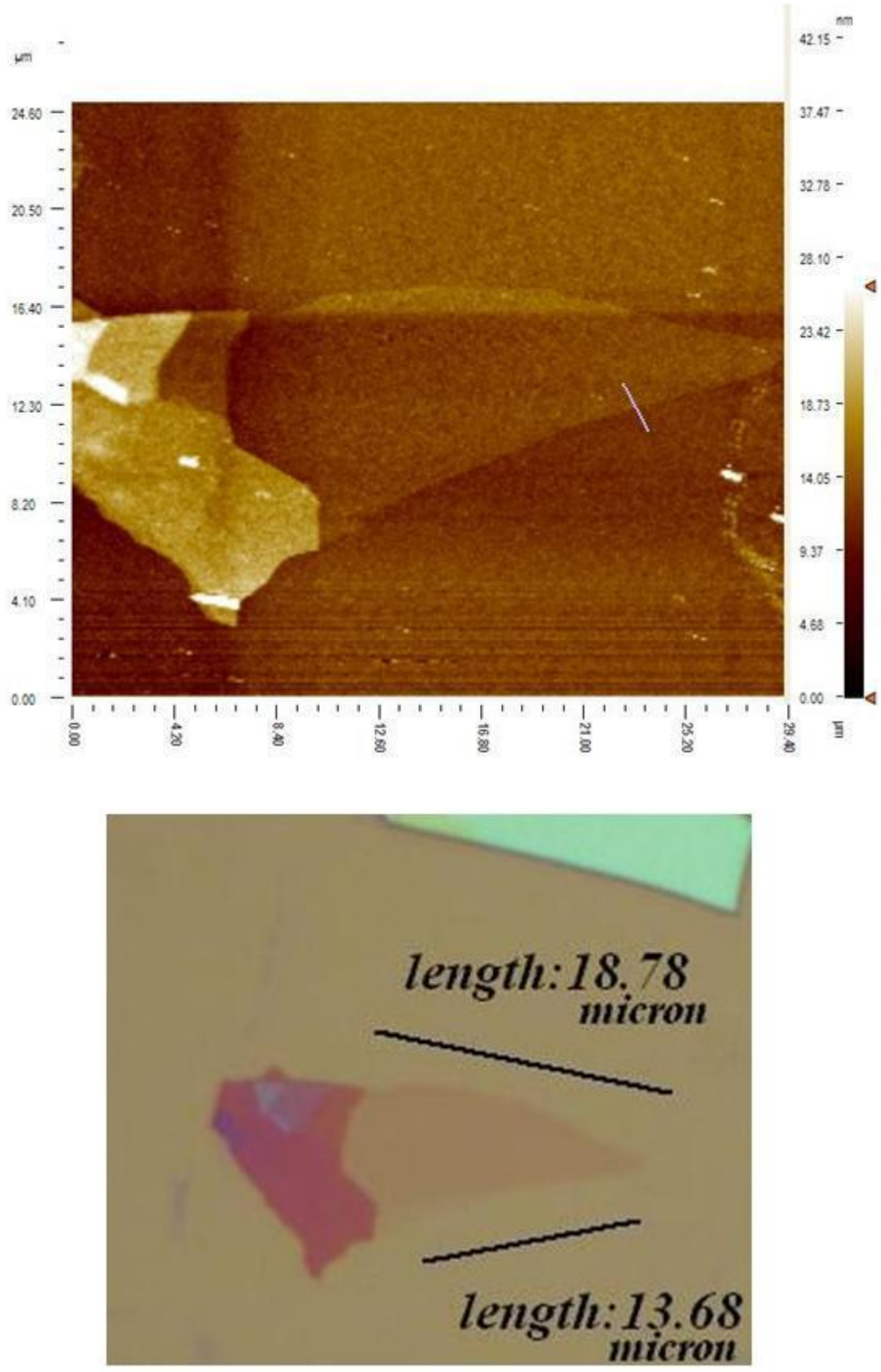

Figure 1.19. (top) Tapping mode AFM image of 3 layer graphene and (bottom) its optical microscope image.

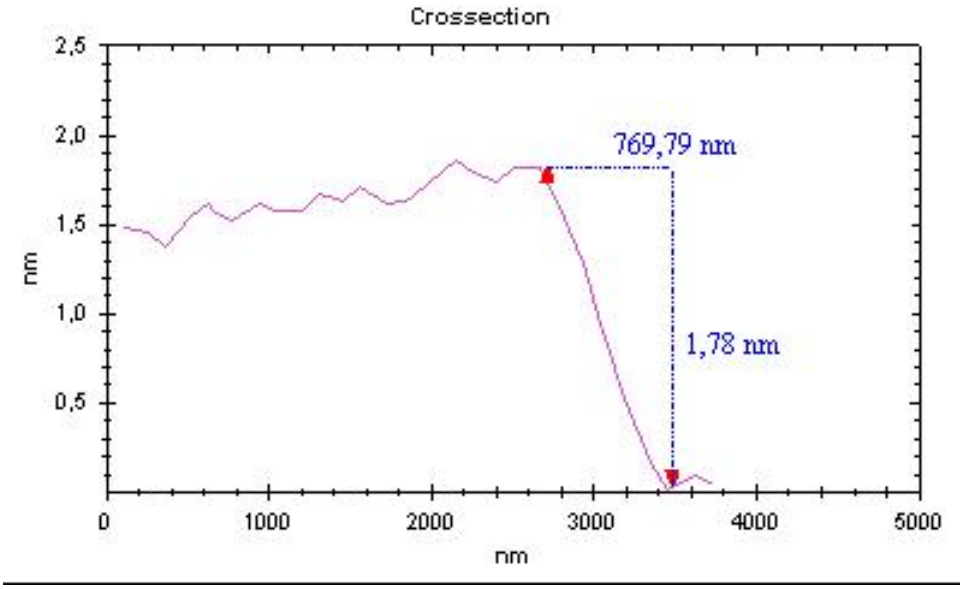

Figure 1.20. Cross section of AFM scan of graphene (see the pink scratch on the Figure 1.19).

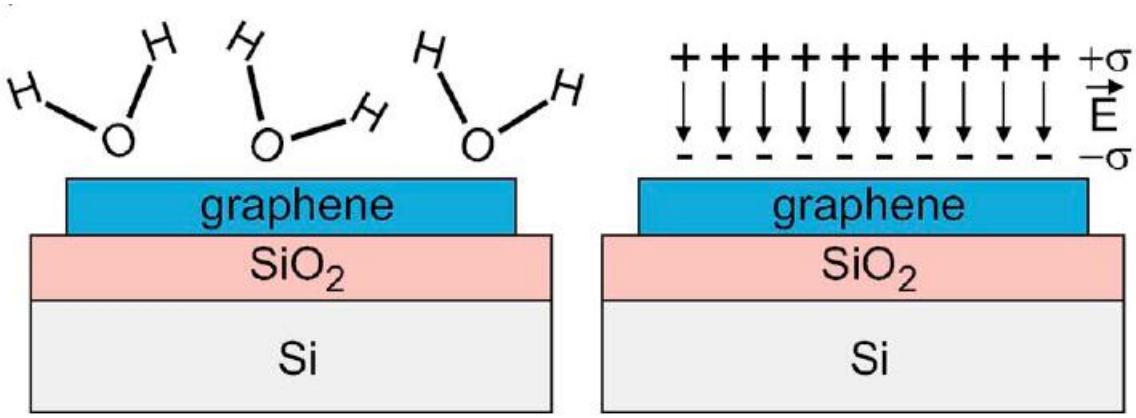

Figure 1.21. Water molecules absorb on the average with the oxygen atom pointing towards the graphene sheet and form a dipole layer with an effective surface charge σ.

1.3.3. Raman Spectroscopy

Graphite has four characteristic Raman peaks which are D, G, D', G' which can be explained using double-resonant Raman scattering [34]. The D peak ($\sim$1,400 cm^{-1}) is related to the finite crystallite size, shows the structural quality and disappears for perfect crystals. The integrated G line signal ($\sim$1,600 cm^{-1}) is correlated with the thickness of the graphitic flake and is shifted upward in frequency for double- and single layer graphene compared to that of bulk graphite. The peak width of D' line ($\sim$2,700cm^{-1}) shows a very strong contrast between single and few layer graphene. It is an overtone of the D peak, where the electron is backscattered by a second phonon instead of a defect. The G' peak ($\sim$3,200 cm^{-1})represents the overbending of longitudinal optical branches of graphite. The intensity of G line versus D' line increases from single layer to double layer graphene layer as seen in Figure 1.22 and Figure 1.23. We examined our graphene flakes with a Renishaw InVia Reflex Raman Microscope System (Renishaw Plc., New Mills, Wottonunder-Edge Gloucestershine, UK) installed at Prof. Dr. Mustafa Çulha's laboratory at Yeditepe University. We used a 514 nm wavelength green argon ion laser with a 25 mW maximum power. 2.5mW laser power is chosen to reduce the heating effect. The numerical aperture of the objective lens was 0.8. We estimate the laser spot size to be around a few micrometers. The data are collected from various parts of the graphene layers as demonstrated in Figure 1.14.

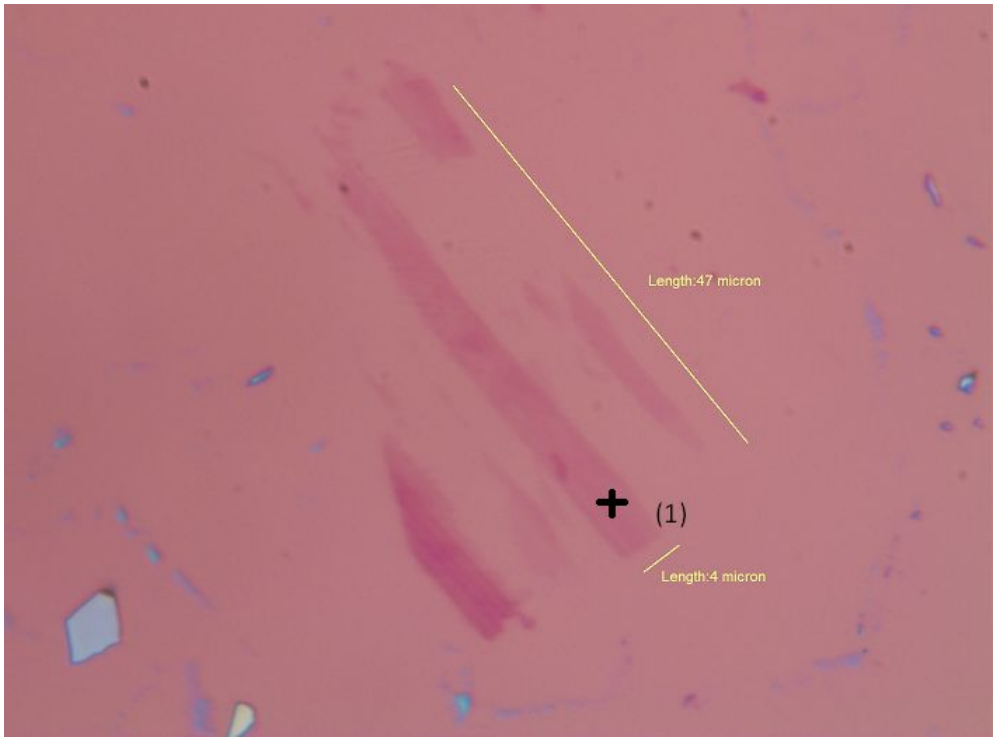

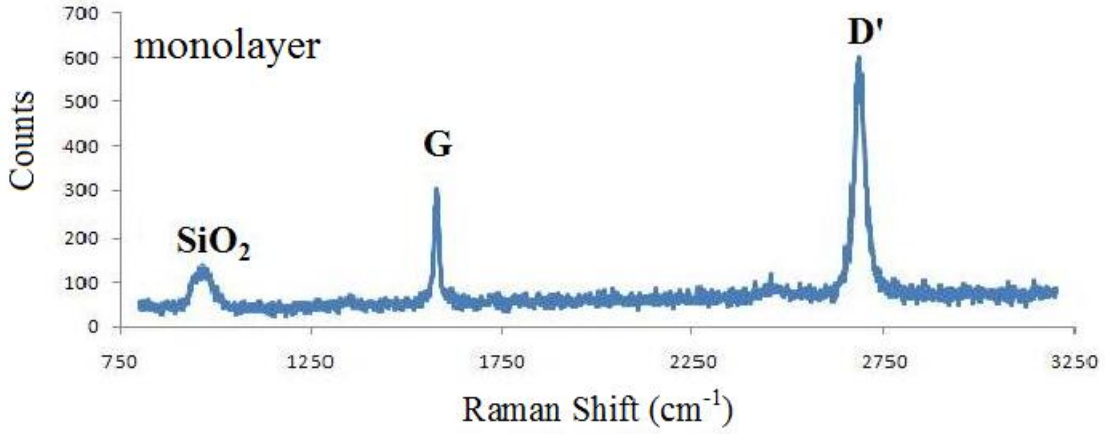

Figure 1.22. Raman spectroscopy of monolayer graphene taken from position (1) in the image above.

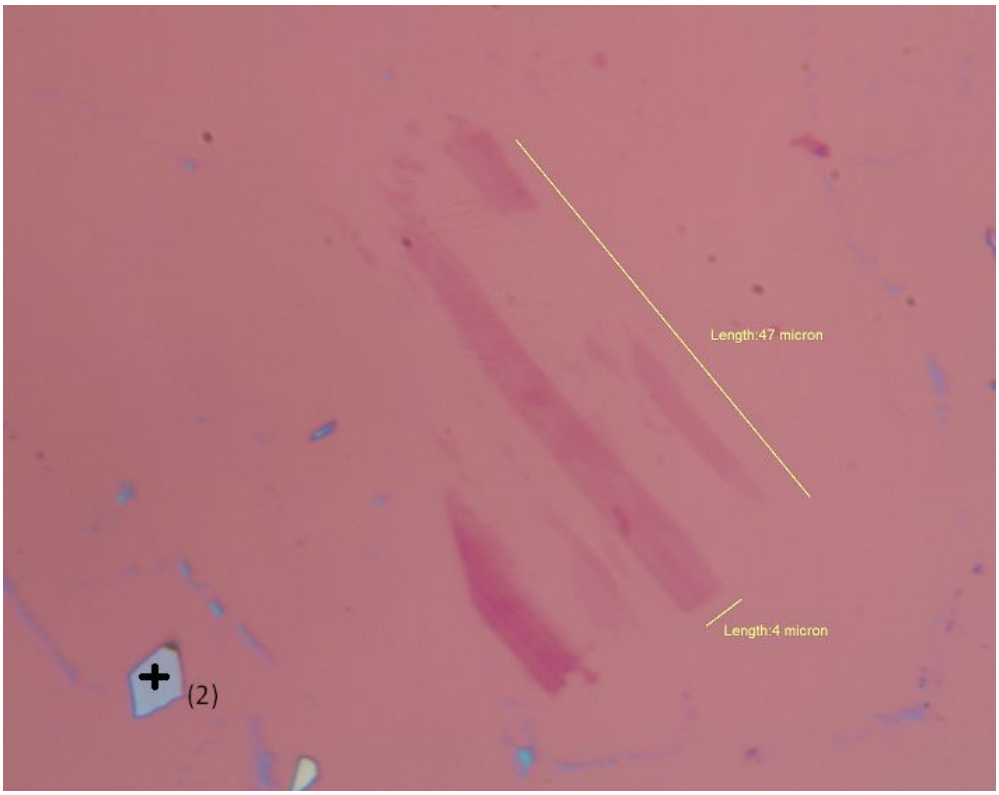

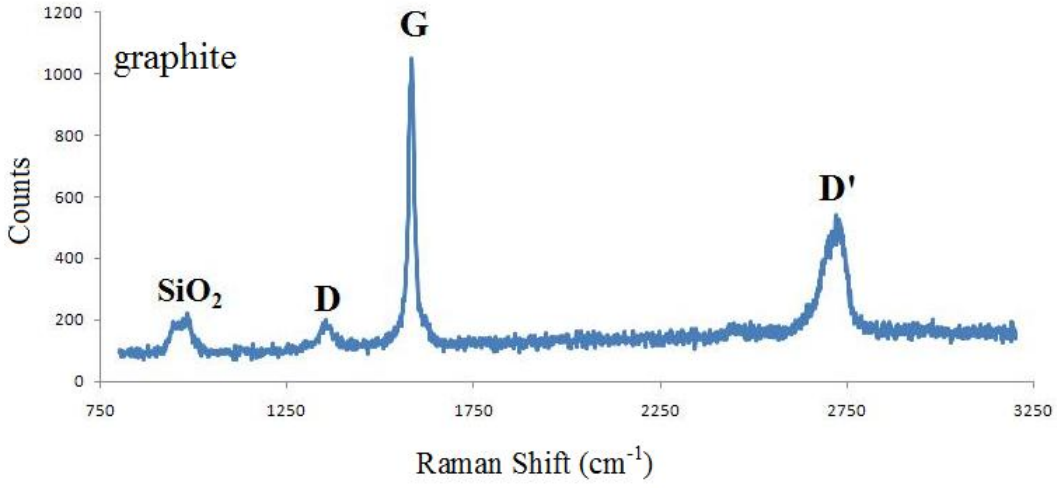

Figure 1.23. Raman spectroscopy of graphite taken from position (2) in the image above.

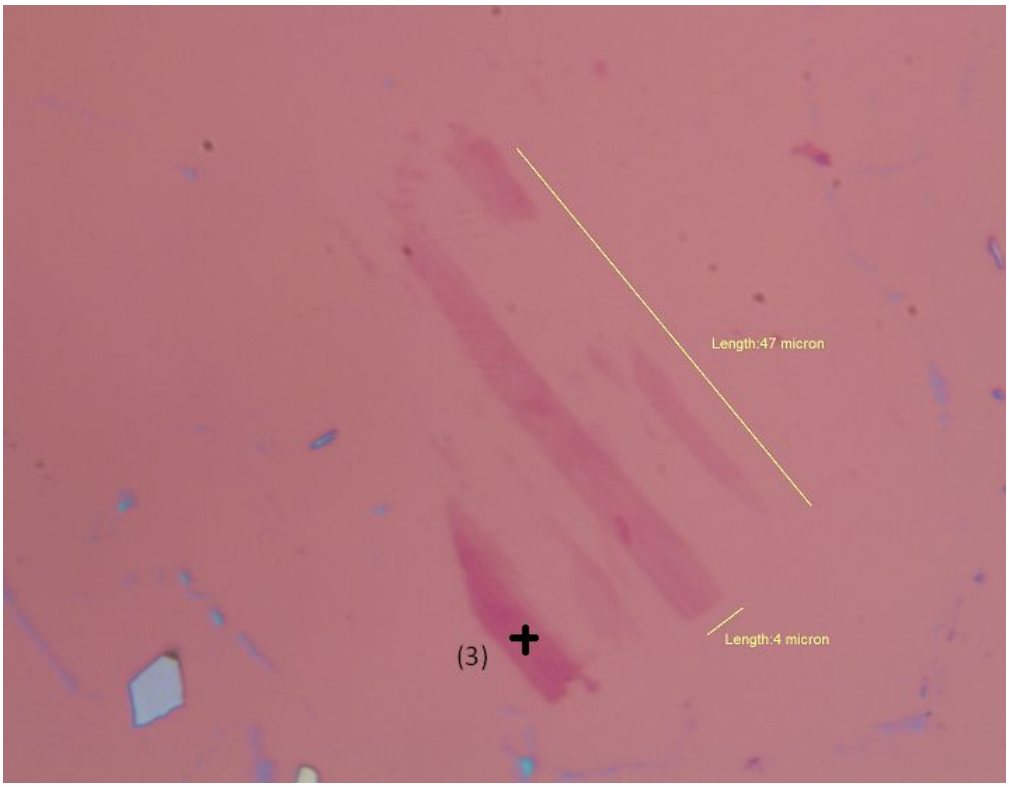

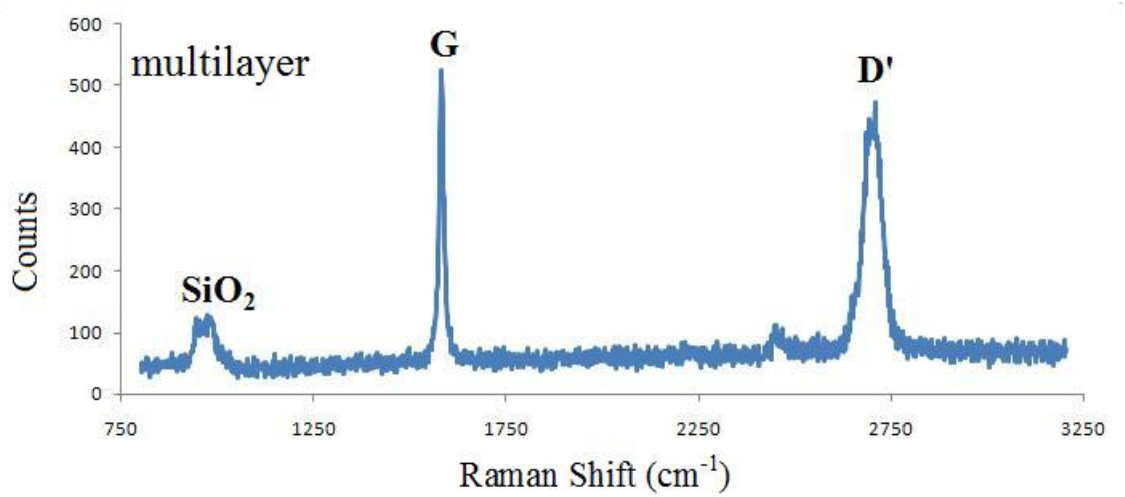

Figure 1.24. Raman spectroscopy of multilayer graphene taken from position (3) in the image above.

2. GRAPHENE BASED TRANSISTOR

The transistor is a three-terminal device, where the current through two terminals can be controlled by small changes made in the current or voltage at the third terminal. This control feature allows us to amplify small AC signals or to switch the device from an *on* to an *off* state and vice versa. These two operations, amplification and switching, are the basic building block of all the electronic circuits.

The field-effect transistor (FET), also called unipolar transistor, relies on electric field control of the conductivity of a semiconductive channel material. In Figure 2.1 I-V curve of an n-type MOSFET is given. The gate voltage, V_G controls the drain current versus drain voltage characteristics, ultimately the value of the drain current at saturation. As the gate voltage increases the saturation drain current increases.

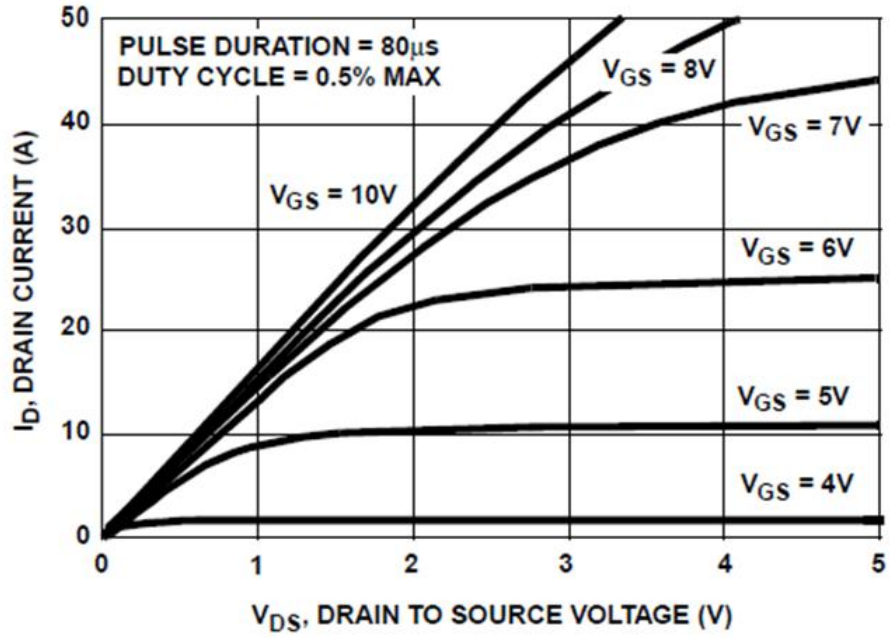

Figure 2.1. The I-V curves of n-type MOSFET IRF540N taken from data sheet, Fairchild Semiconductor Inc.

Silicon has been used for transistors for years and through miniaturization of devices, higher speeds and lower power consumption have been realized. However, in recent years, miniaturization technology has almost approached its limits. Achieving

further improvements, higher performance is becoming increasingly more difficult. This has led to active research on next-generation transistors using alternative materials such as III-V's, carbonanotubes, nanotubes and ***graphene*** as channel materials. However, no realistic candidates has emerged yet.

Graphene conducts electricity faster than most materials since electrons can travel through straight lines between the carbon atoms without being scattered. This means faster and more efficient electronic components that also require less power.

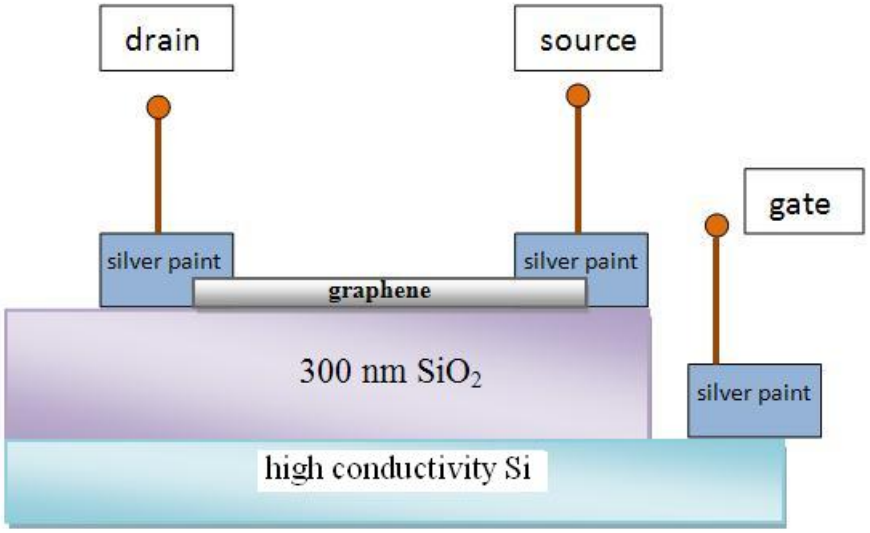

Figure 2.2. The device layout of graphene FET.

We fabricated a graphene FET using silver paint as drain and source contacts. The reason of not using the lithographical techniques is that the electron lithography (e-beam) and optical lithography facilities at SabancıUniversity were not in reliably operating conditions to achieve the desired results in a very limited amount of time. The optical lithography system at Sabancı University clean room has an alignment resolution of around 20 microns, which is unsuitable for production of graphene based electronic devices. Sabancı University e-beam system, which is composed of a Zeiss Gemini FEG SEM & Nabity Pattern Generator has much better resolution, 20 nm to 50 nm. However, the system could not be calibrated in time, for this study, due to prolonged problems at the SEM itself. We will produce our graphene based devices in the future, using this e-beam lithography system in two steps. First, the coordinates of

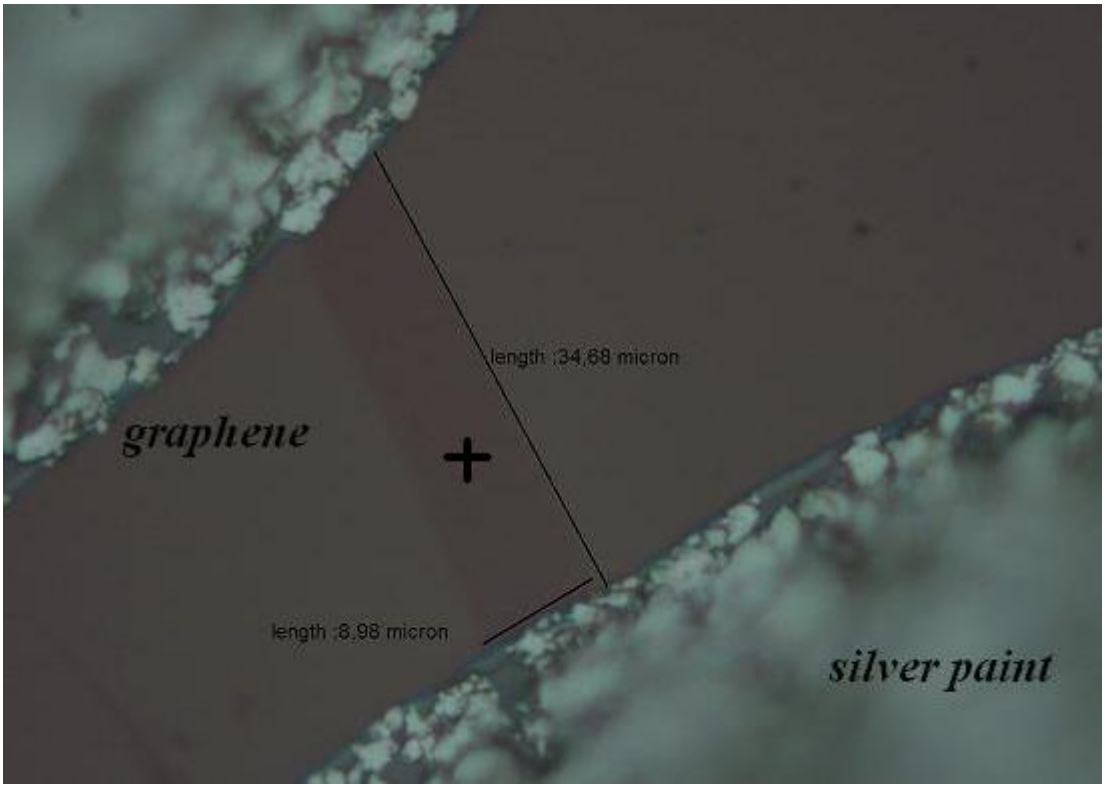

Figure 2.3. The silver paint contacts taken from multi layer graphene sheet. The length and the width of source-drain region is ∼35 μm and ∼9 μm, respectively.

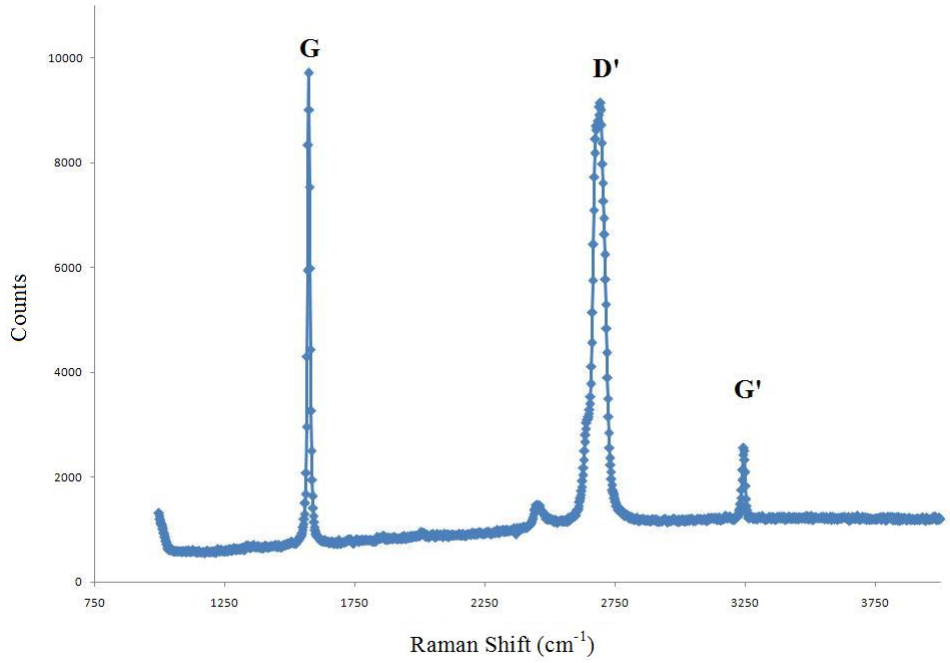

Figure 2.4. The Raman Spectroscopy of graphene FET taken from the marked point. From this spectrum we can interpret that this is a 2-3 layer sheet. (obtained using Nicolet Almega XR Raman Spectrometer at SANAEM, Ankara)

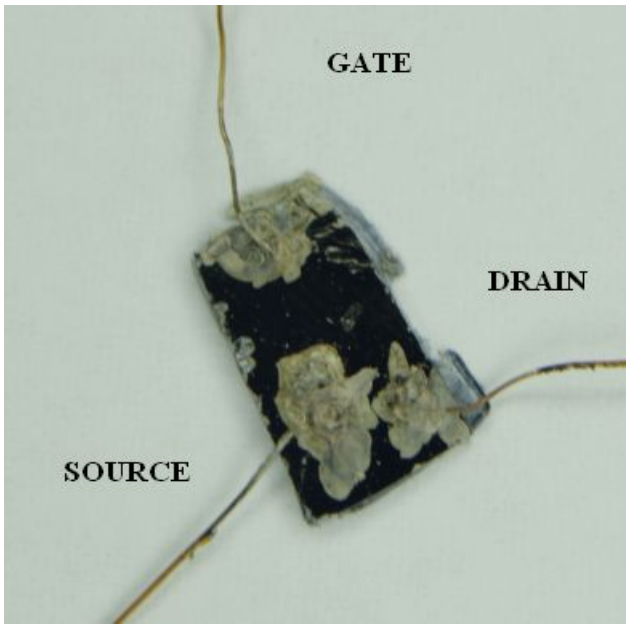

Figure 2.5. The picture of graphene FET device.

graphene will be determined under optical microscope accurately. After that, the wafer will be covered by an e-beam resist (PMMA). Large contact pads will be patterned with e-beam lithography and Ti/Au lift-off, approximately aligning them near the graphene flake. Ti/Au contacts will be used to obtain electrical contacts from graphene. Then these contact pads will be measured accurately again under the optical microscope and the Ti/Au contacts to the graphene layer will be deposited directly on the graphene using e-beam lithography under SEM guidance. The large metal contact pads deposited at the first step will still be visible under the PMMA resist in SEM.

Electrical characterization of the graphene FET has been carried out at room temperature. p-type Phosphorus or Boron doped Si(100) wafers with 300nm thick wet thermal oxides on both sides are used for substrate. The wafer had a resistivity of 0.001-0.005 Ω-cm. We used SPI SafeShip^{TM} Non-flammable Silver Paint to make contacts on graphene layers. Contacts are painted under optical microscope by hand with the help of a toothpick (see Figure 2.3). The silicon chips were fixed on microscope glass slides by using PMMA (Poly(methyl methacrylate)) which is the polymer used as resist for e-beam lithography. Then, the graphene layer's position is determined with the optical microscope with ×50 objective lens. It is not efficient to use a lower magnification to detect single layer graphene. There are no lithographical steps used

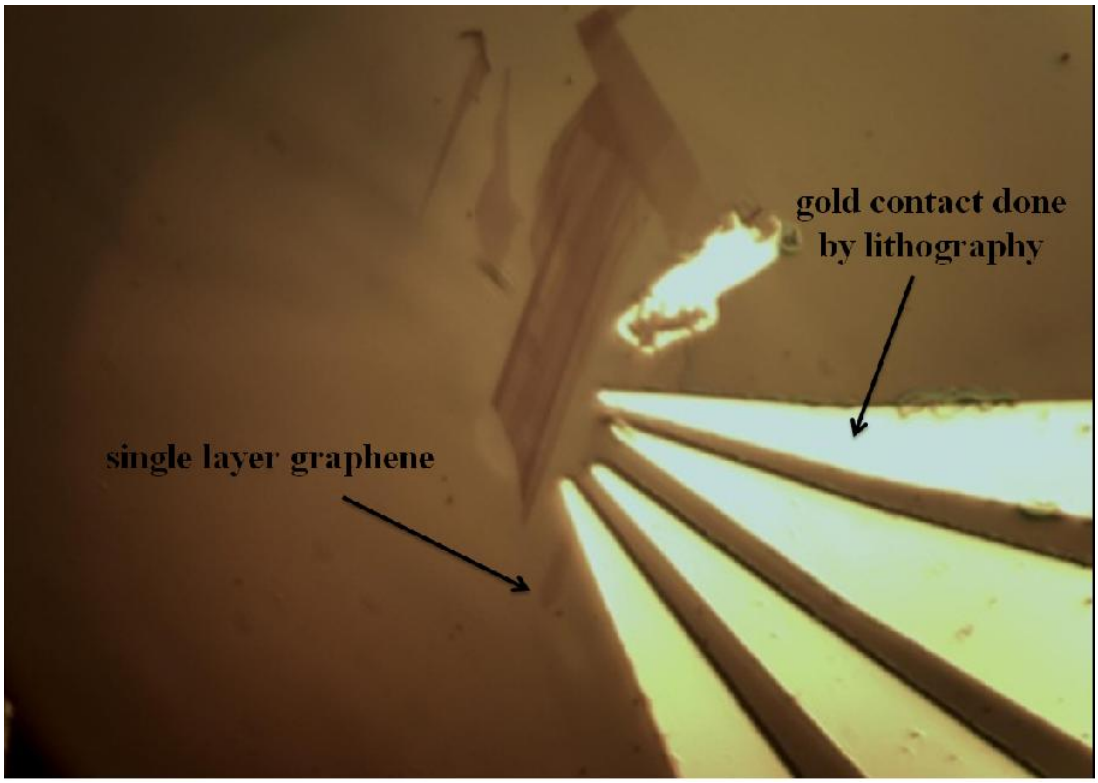

Figure 2.6. Gold contacts are obtained by optical lithography method (courtesy of Dr. Hidayet Çetin).

during this process. Unfortunately, it was very hard to have a successful result with this method. The yield of this process was very low and we have used up many big pieces of graphene layers. Out of 30 trials we managed to make one successful graphene FET. The I-V curves are measured by Keithley 2612 System SourceMeter and the data are acquired by using the LabTracer 2.0 software supplied by Keithley.

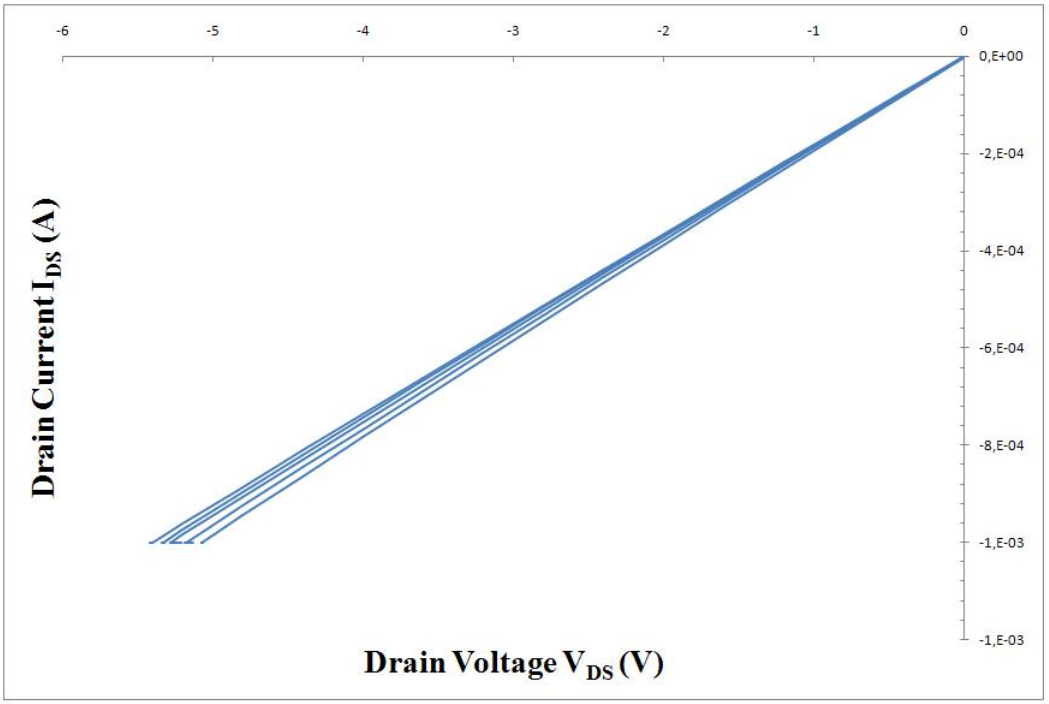

Figure 2.7. I_{DS}-V_{DS} curves of graphene based FET. V_G=−20/20 V (in 5 steps) with a compliance of 0,01 A.

Figures 2.7, 2.8 and 2.9 shows the I_{DS}-V_{DS} curves of graphene FET acquired with LabTrace 2.0 software and Keithley 2612 System SourceMeter. The slopes of the curves give the channel resistance measurement.

We have calculated the resistance of the graphene layer between 5,550±210 Ω and the sheet resistance as $17\pm2\times10^{18}$ Ω/cm^2. The length and the width of source-drain region are $\sim$ 35 μm and $\sim$ 9 μm respectively. The resistivity is calculated to be between $4.1\pm0.2\times10^{-5}$ Ω.cm, which is the half of the resistivity in literature (see Section 1.1.2). Here we assumed the graphene layer's thickness as 2 or 3 out of the Raman Spectroscopy.

One advantage of graphene FET is that it can act as n- or p-type FET at the same time, see Figure 2.8 and 2.9. Graphene shows ambipolar channel characteristics, in other words, it does not have a physically determined primary carrier type and can function as n-type or p-type material, depending on the polarity of the gate voltage. In comparison to MOSFET, graphene FET does not have a saturation (active) region but only linear (Ohmic) region. It has linear I_{DS} vs. V_{DS} curves.

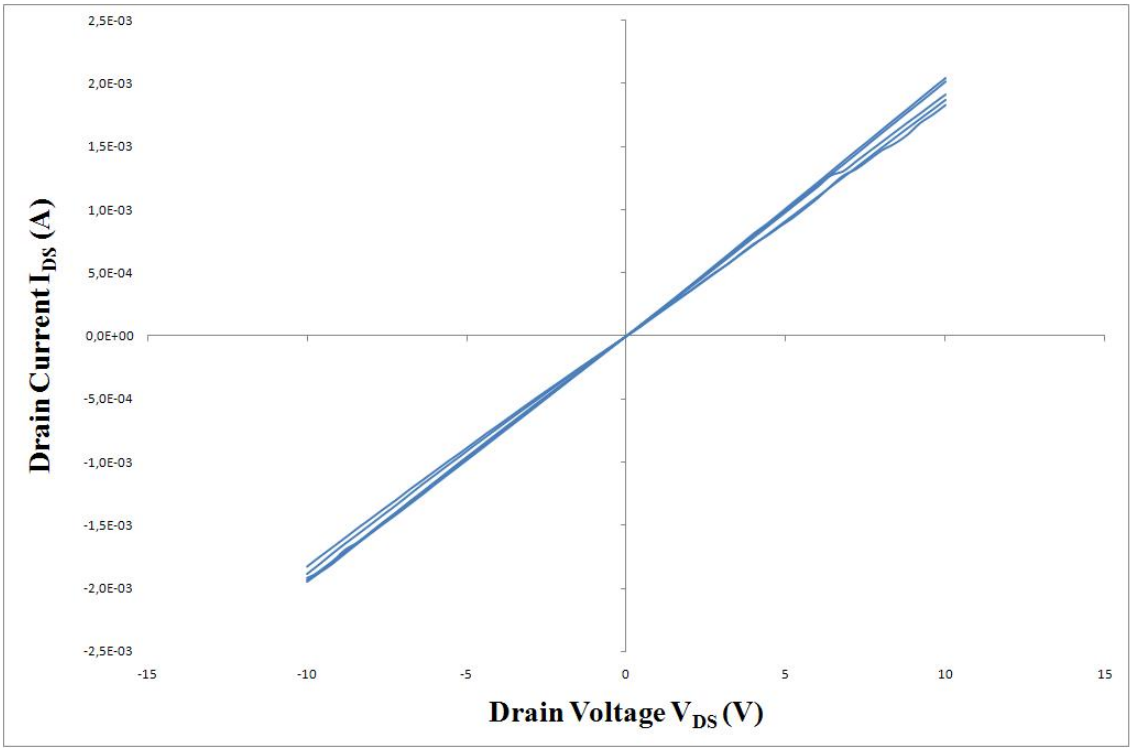

Figure 2.8. I_{DS}-V_{DS} curves of graphene based FET. V_G=−20/20 V (in 5 steps) with a compliance of 0,01 A.

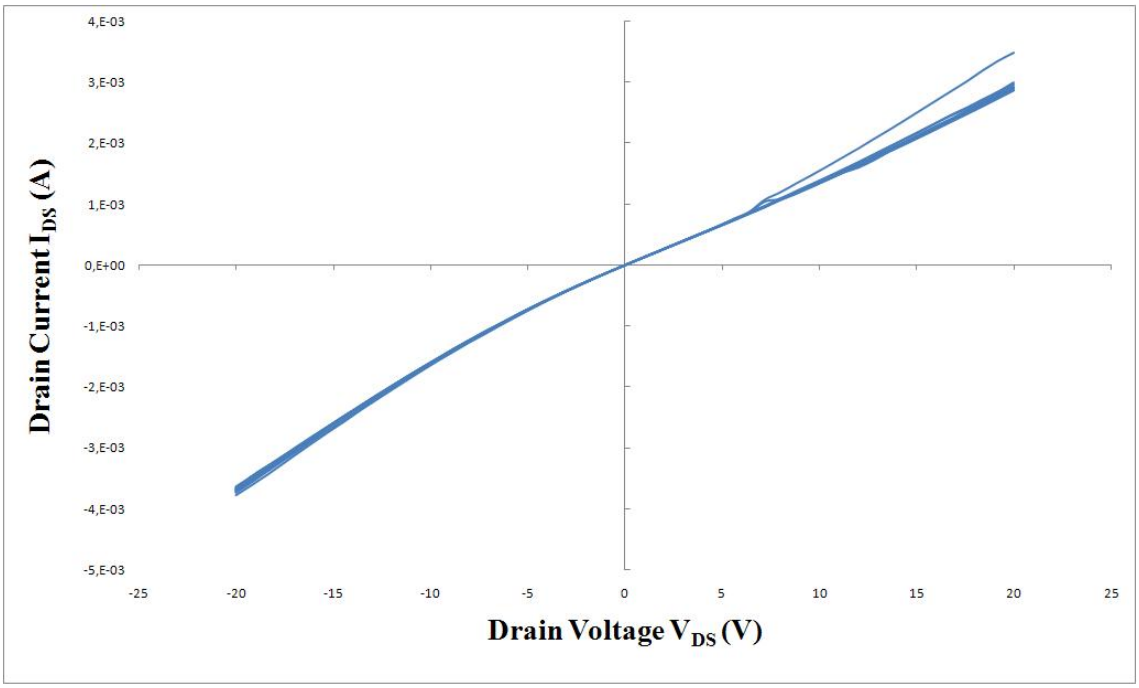

Figure 2.9. I_{DS}-V_{DS} curves of graphene based FET. V_G=−20/20 V (in 10 steps) with a compliance of 1,5 A.

n-type or p-type conductance is measured as a function of gate voltage, V_{SG}. A perfect ambipolar conductor would have a transition from p to n type at V_G=0 but the presence of atmospheric water vapor provides a small doping effect, which biases the channel slightly [33]. In our experiment, this shift is around $-4V/-6V$ as can be seen in Figures 2.10 to 2.17. Keeping the sample in air and forming the Ohmic contacts with silver paint might have resulted in such a big voltage shift. The humidity in the environment might have had a role in this shift too.

In Figures 2.10, 2.11, 2.12, 2.13,2.14 2.15, 2.16, 2.17, the drain-source current I_{DS} versus gate-source voltages V_{GS}, are displayed for different drain-source V_{DS} voltages. We observed that the curves are reflected as the drain voltage gets is reversed as expected. This reflection is not observed after $|V_{DS}|\geq 7V$.

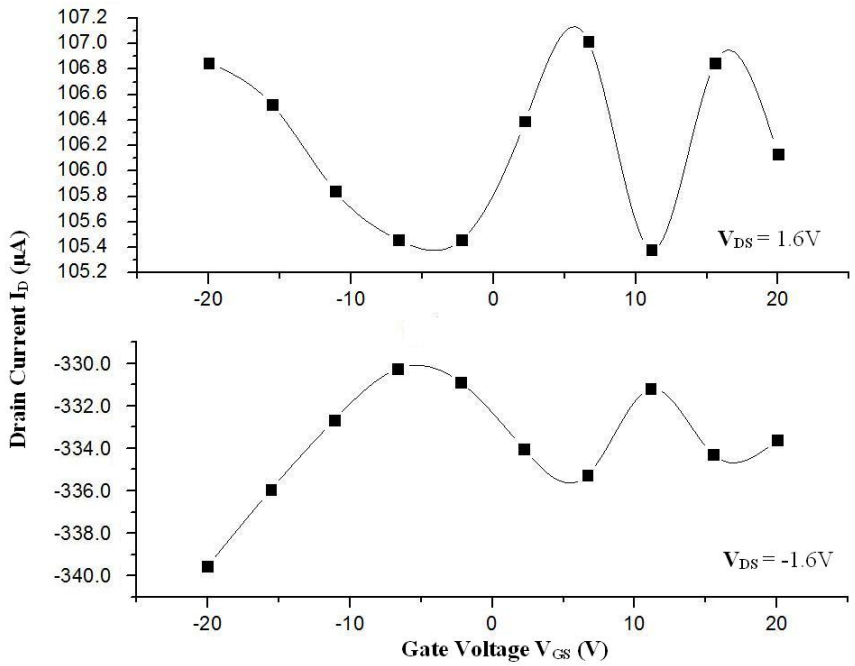

Figure 2.10. I_{DS} vs V_{GS} curve of graphene FET for 1.6 V and -1.6 V drain voltage.

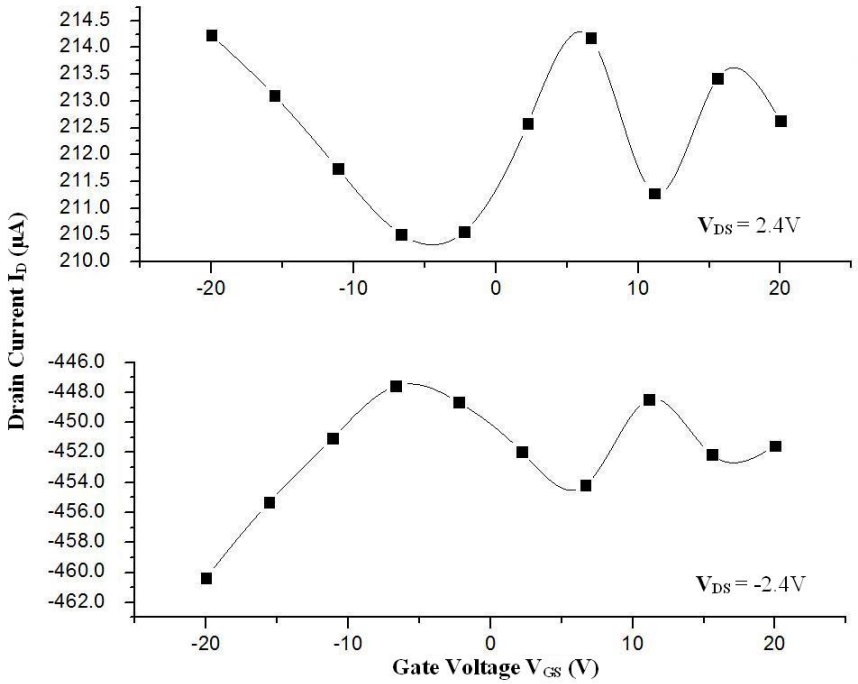

Figure 2.11. I_{DS} vs V_{GS} curve of graphene FET for 2.4 V and -2.4 V drain voltage.

The minimum position of is drain current is shifted from V_{GS}=$-$4V to V_{GS}=$-$7V as one changes the drain voltage from +1.6V to +4.8V. The drain current makes a peak around $V_{GS}\simeq$6-7V and then makes a dip around $V_{GS}\simeq$11V. After around $|V_{DS}|\geq$7V,

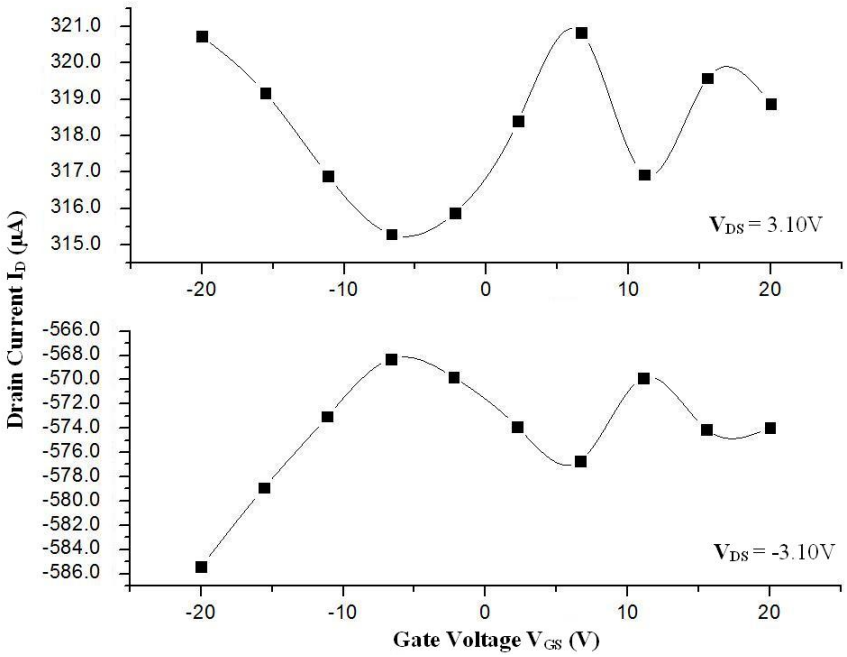

Figure 2.12. I_{DS} vs V_{GS} curve of graphene FET for 3.10 V and −3.10 V drain voltage.

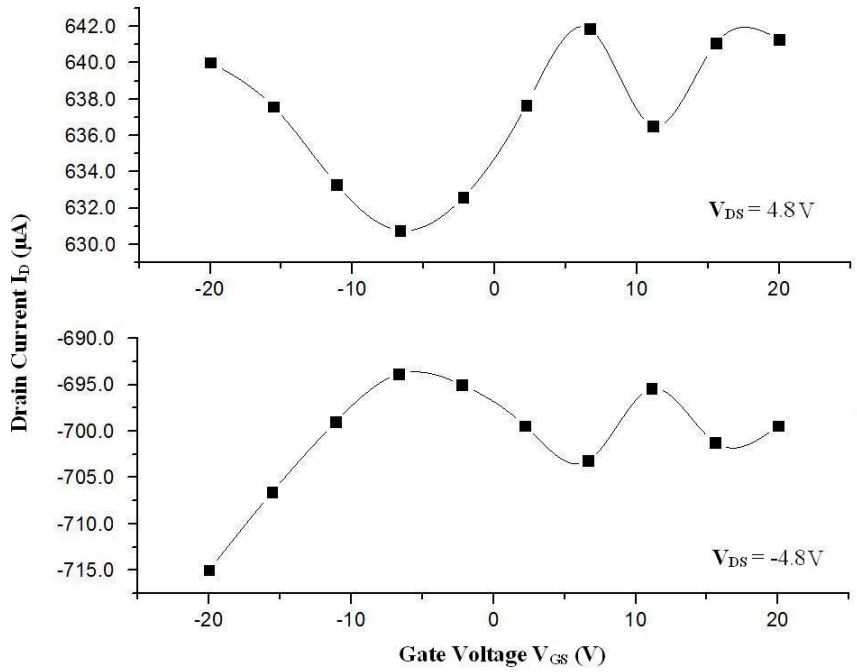

Figure 2.13. I_{DS} vs V_{GS} curve of graphene FET for 4.8 V and −4.8 V drain voltage.

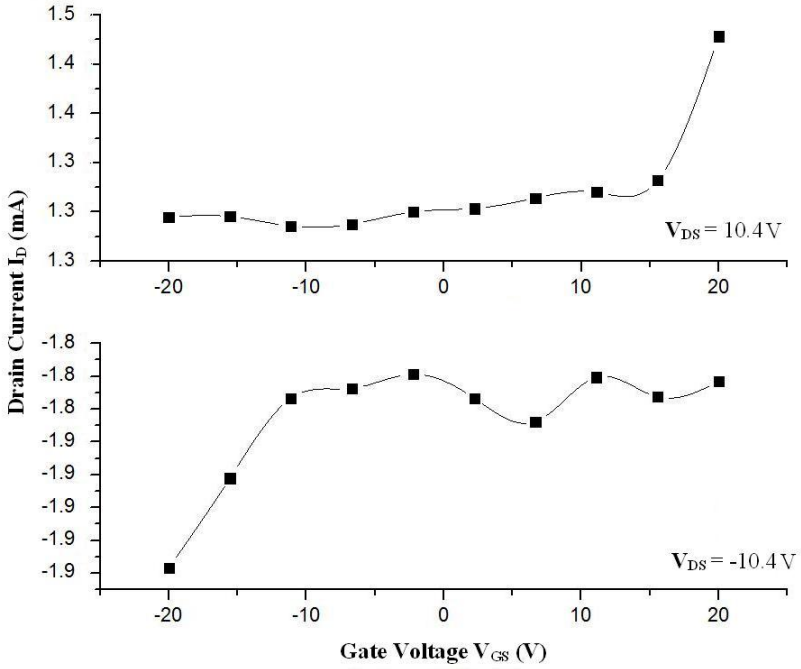

Figure 2.14. I_{DS} vs V_{GS} curve of graphene FET for 10.4 V and −10.4 V drain voltage.

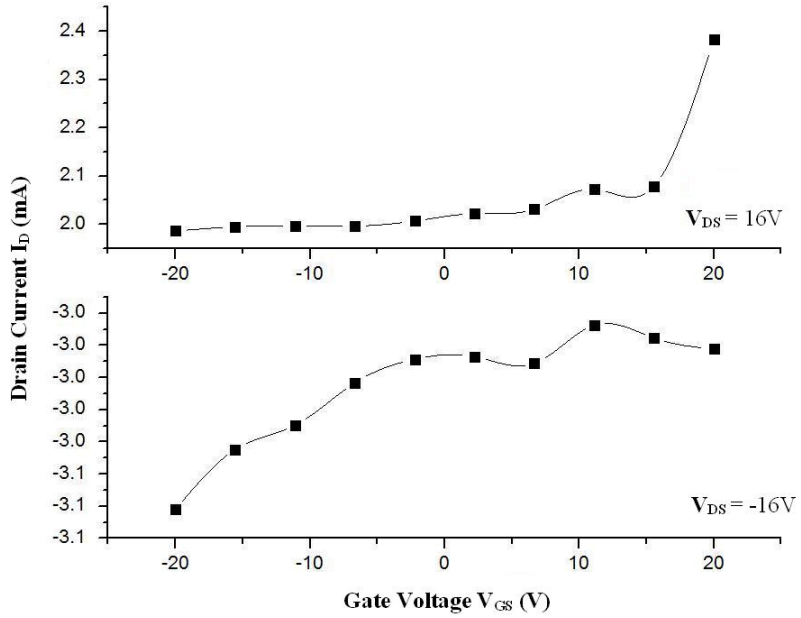

Figure 2.15. I_{DS} vs V_{GS} curve of graphene FET for 16 V and −16 V drain voltage.

the I_{DS}-V_{GS} curves become more nonlinear as can be seen in Figure 2.14 - 2.17. Another I_{DS} vs V_{GS} curve obtained on the same graphene transistor on another day is shown in Figure 2.18.

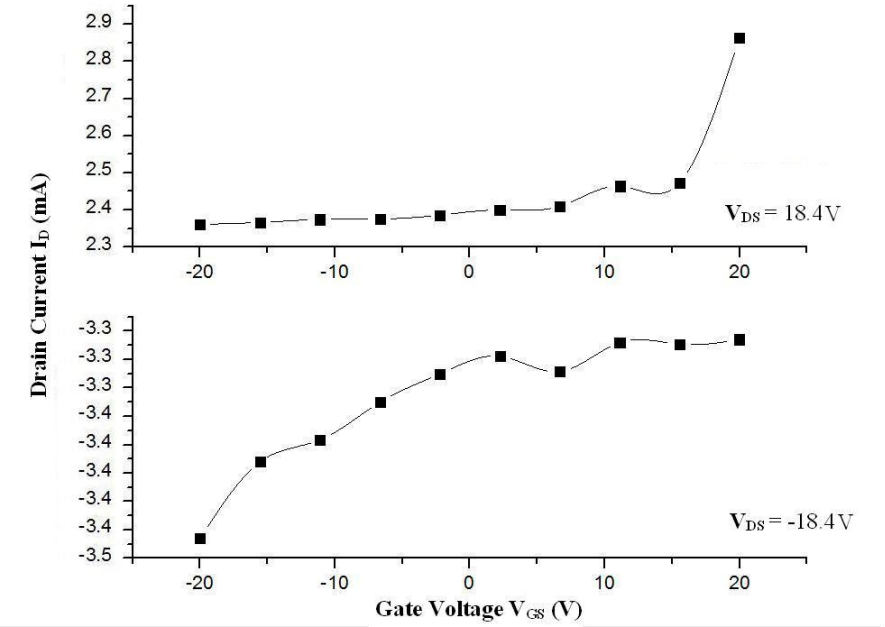

Figure 2.16. I_{DS} vs V_{GS} curve of graphene FET for 18.4 V and -18.4 V drain voltage.

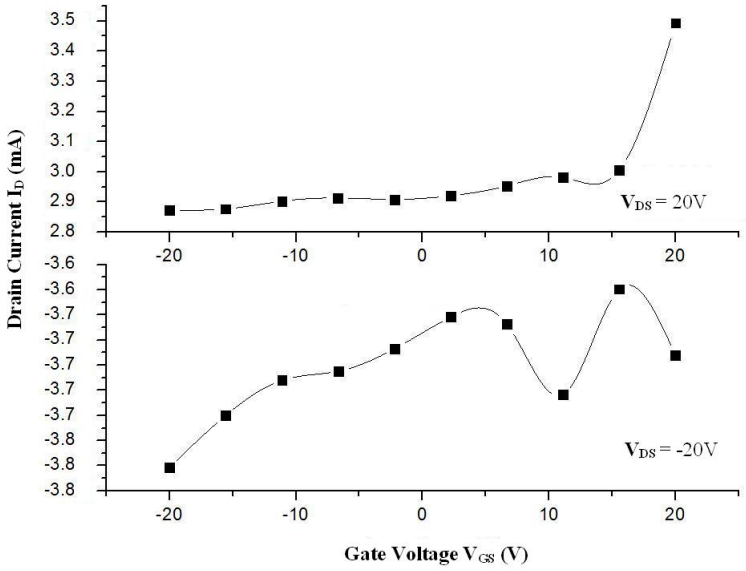

Figure 2.17. I_{DS} vs V_{GS} curve of graphene FET for 20 V and -20 V drain voltage.

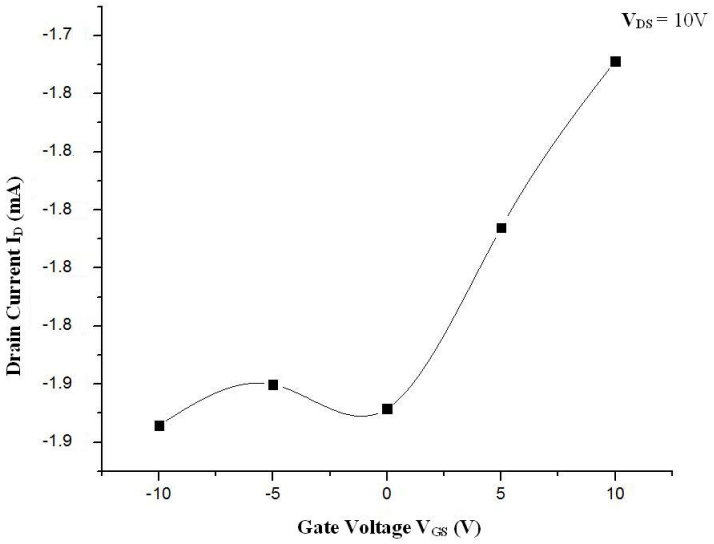

Figure 2.18. I_{DS} vs V_{GS} curve of graphene FET at V_{DS}=10 V.

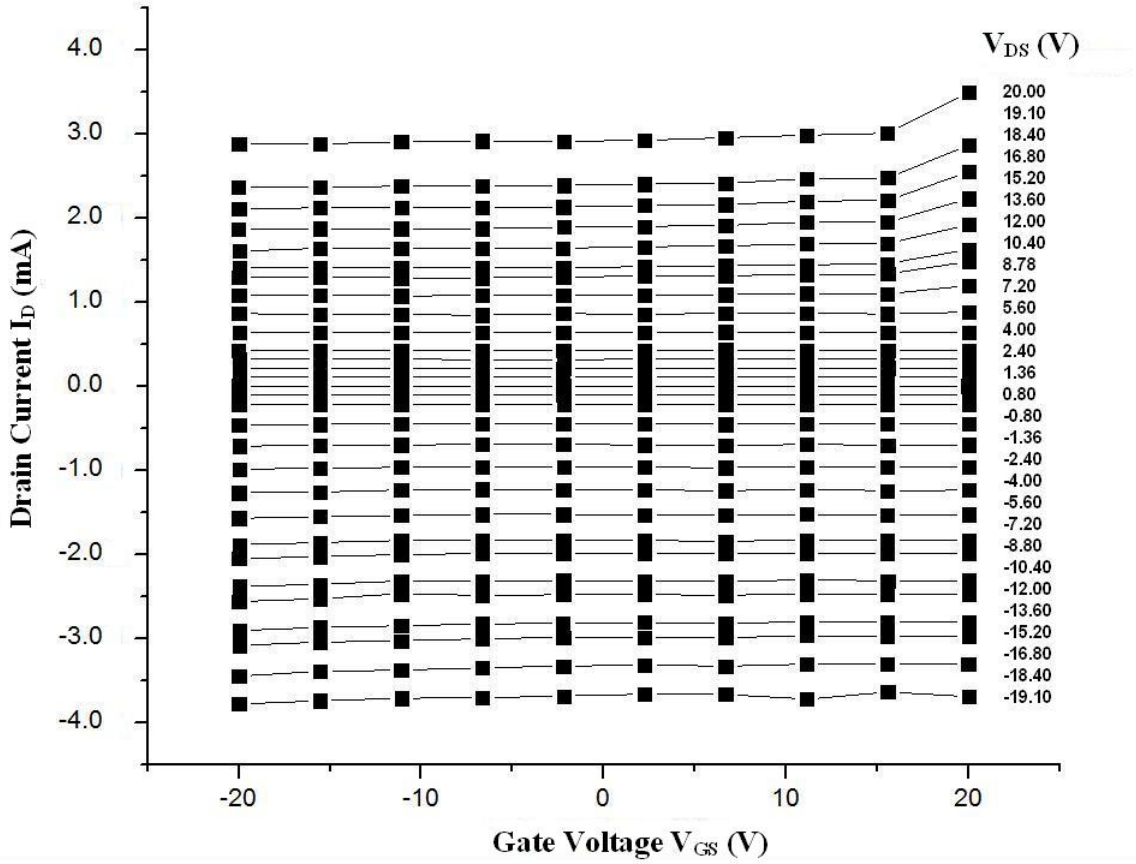

Figure 2.19. I_{DS} vs V_{GS} curves of graphene FET for different drain voltages.

Figure 2.19 summarizes all of our I_{DS}-V_{GS} curves for a range of V_{DS} voltages.

3. CONCLUSION

We investigated the production methods and characterization of single and multilayer graphene sheets. Mechanical exfoliation of single and multilayer graphene has been successfully demonstrated during this thesis work. We have also attempted to produce graphene sheets with chemical decomposition using solvents like DMF, but we have failed. Moreover, we have started epitaxial growth of graphene on SiC(1000) surface, but we have not achieved considerable progress. We have only managed to characterize the bare SiC(1000) surface using AFM. Mechanical exfoliation with Scotch tape has been found to be the easiest and the cheapest of all the methods that we have tried.

The mechanical exfoliation method provides pristine graphene sheets, which are easily identified under optical microscope. The number of layers can also be identified reliably after a training time. Unfortunately, graphene produced by mechanical exfoliation method is not an efficient method for mass production. However, Chemical Vapor Deposition (CVD) growth of graphene on metals and epitaxial growth of graphene on silicon carbide wafers have also drawbacks. During these processes, it is not possible to produce suspended graphene layer on the substrate and the electrical properties are usually much worse than the graphene sheets produced by mechanical exfoliation method.

Hybridization between the d-orbitals of the substrate atoms and π-orbitals of graphene significantly alters the electronic structure of the epitaxial graphene. Moreover, the CVD method using a metallic catalyst has a major advantage; the graphene can be formed on any substrate. Unfortunately, it is impossible to build transistors on conductive metal substrates. Therefore, the graphene that had been formed on the metal surface has to be transferred to an insulating substrate to produce electronic devices.

We have successfully characterized the graphene layer that we produced by optical and Atomic Force Microscopy(AFM). The graphene sheets are further characterized by micro Raman Spectroscopy and we could verify the single and multilayer graphene sheets by an alternative method.

We have also fabricated a graphene field effect transistor by using *"manolithography"*, manually painting contacts using silver paste and a toothpick! Even though the yield was terribly low, ∼3%, we successfully operated our graphene FET at room temperature and obtained its electrical characteristics using a Keithley Sourcemeter.

In conclusion, we have produced single and multilayer graphene sheets using mechanical exfoliation method and fabricated a graphene FET within the scope of a masters thesis in Turkey for the first time. Graphene is a promising material, which offers large variety of application possibilities from FETs to nano-sensors (gas sensors, magnetic sensors, etc.). Our future work will focus on to produce a 10 nm nano-Hall sensor by using single and multilayer graphene sheets and achieve better spatial and magnetic resolution in Scanning Hall Probe Microscopy and Gradiometry, utilizing graphene's marvelous electronic properties. We hope that low electron density and high electron mobility of graphene, even at room temperature, will yield a much higher magnetic resolution. It seems that even smaller Hall sensors (<10nm) are possible to fabricate using graphene sheets.

REFERENCES

1. Landau L. D., "Zur Theorie der Phasenumwandlungen II", Phys. Z. Sowjetunion, Vol. 11, pp. 26-35, 1937.

2. Landau L. D. and E. M. Lifshitz, "Statistical Physics Part I", Sections 137 and 138, Pergamon, Oxford, 1937.

3. Peierls R. E., "Bemerkunghen über Umwandlungstemperaturen", *Helv. Phys. Acta*, Vol. 7, pp. 81-83, 1934.

4. Peierls R. E., "Quelques proprietes typiques des corpes solides", *Ann. Inst. Henri Poincare*, Vol. 5, pp. 177-222, 1935.

5. Born M. and K. Huang, "Dynamical Theory of Crystal Lattices", Clarendon, Oxford 1954.

6. Mermin N. D., "Crystalline Order in Two Dimensions", *Phys. Rev.*, Vol. 176, pp. 250-254, 1968.

7. Mermin N. D. and H. Wagner, "Absence of Ferromagnetism or Antiferromagnetism in One- or Two-Dimensional Isotropic Heisenberg Models", *Phys. Rev. Lett.*, Vol. 17, pp. 1133-1136, 1966.

8. Novoselov K. S. *et al.*, "Two-dimensional atomic crystals", *PNAS*, Vol. 102, pp. 10451-10453, 2005.

9. Meyer J. C., Geim A. K., Katsnelson M. I., Novoselov K. S., Booth T. J., Roth S., "The structure of suspended graphene sheets", *Nature*, Vol. 446, pp. 60-63, 2007.

10. Dresselhaus G. *et al.*, "Science of Fullerenes and Carbon Nanotubes", Academic Press 1996.

11. Geim A. K. and K. S. Novoselov, "The rise of graphene", *Nature Materials*, Vol. 6, pp. 183-191, 2007.

12. Novoselov K. S. *et al.*, "Two-dimensional gas of massless Dirac fermions in graphene", *Nature*, Vol. 438, pp. 197-200, 2005.

13. Chen, J. H. *et al.*, "Intrinsic and Extrinsic Performance Limits of Graphene Devices on SiO_2", *Nature Nanotechnology*, Vol. 3, pp. 206-210, 2008.

14. Novoselov K. S. *et al.*, "Unconventional quantum Hall effect and Berry's phase of 2π in bilayer graphene", *Nature Physics*, Vol. 2, pp. 177-180, 2006.

15. Chen J. H., C. Jang, C. Adam, M. S. Fuhrer, E. D. Williams and M. Ishigami, "Charged-Impurity scattering in graphene", *Nature Physic*s, Vol. 4, pp. 377-381, 2008.

16. Schedin F., A. K. Geim, S. V. Morozov, E. W. Hill, P. Blake, M. I. Katsnelson, K. S. Novoselov, "Detection of individual gas molecules adsorbed on graphene", *Nature Materials*, Vol. 6, pp. 652-655, 2007.

17. Balandin A.A., S. Ghosh, W. Bao, I. Calizo, D. Teweldebrahn, F. Miao, and Lau C.N., "Superior Thermal Conductivity of Single-Layer Graphene", *Nano Letters*, Vol. 8, pp. 902-907, 2008.

18. Mingo N., D. A. Broido, "Carbon Nanotube Ballistic Thermal Conductance and Its Limits", *Physical Review Letters*, Vol.95, pp. 096105-096110, 2005.

19. Mingo N. and D.A. Broido, "Carbon Nanotube Ballistic Thermal Conductance and Its Limits", *Physical Review Letters*, Vol. 95, pp. 125-130, 2005.

20. Mounet N. and N. Marzari, "First-principles determination of the structural, vibrational and thermodynamic properties of diamond, graphite, and derivatives", *Physical Review B*, Vol. 71, pp. 435-440, 2005.

21. Teo G. *et al.*, "Visibility Study Of Graphene Multilayer structures", *Journal of Applied Physics*, Vol.103, pp. 124302-124310, 2008.

22. Geim A. K. *et al.*, "Making Graphene Visible", *Applied Physics Letters*, Vol. 91, pp. 063124-063128, 2007.

23. Klitzing K. von, G. Dorda, M. Pepper, "New Method for High-Accuracy Determination of the Fine-Structure Constant Based on Quantized Hall Resistance", *Phys. Rev. Lett.*, Vol. 45, pp. 494497, 1980.

24. Hass J., W. A. de Heer and E. H. Conrad, "The growth and morphology of epitaxial multilayer graphene", *J. Phys. Condens. Matter*, Vol. 20, pp. 27-34, 2008.

25. Sutter P.W., J. Flege and E. A. Sutter, "Epitaxial graphene on ruthenium", *Nature Materials*, Vol. 7, pp. 406-411, 2008.

26. Kim K. S., *et al.*, "Large-scale pattern growth of graphene films for stretchable transparent electrodes", *Nature*, Vol. 457, pp. 7230-7235, 2009.

27. Li X. *et al.*, "Large-Area Synthesis of High-Quality and Uniform Graphene Films on Copper Foils", *Science*, Vol. 324, pp. 1312-1320, 2009.

28. Tung V. C., M. J. Allen, Y. Yang and R. B. Kaner, "High-throughput solution processing of large-scale graphene", *Nature Nanotechnology*, Vol. 4, pp. 25-29, 2009.

29. Choucair, M. "Gram-scale production of graphene based on solvothermal synthesis and sonication", *Nature Nanotechnology*, Vol. 4, pp. 30-33, 2008.

30. Hernandez Y. *et al.*, "High-yield production of graphene by liquid-phase exfoliation of graphite", *Nature Nanotechnology*, Vol. 3, pp. 563-568, 2008.

31. Graphene Industries Inc., http://grapheneindustries.com/?Sample+Catalog, 2007

32. Moser J., A. Verdaguer, D. Jimanez, A. Barreiro and A. Bachtold, "The environ-

ment of graphene probed by electrostatic force microscopy", *Applied Physics Letters*, Vol.92, pp. 123507-123510, 2008.

33. Novoselov K. S. *et al.*,"Electric Field Effect in Atomically Thin Carbon Films", *Science*, Vol. 306, pp. 666-680, 2004.

34. Reich S. and C. Thomsen, "Raman Spectroscopy Of Graphite", *Philos. Trans. R. Soc. London, Ser. A*, Vol. 2271, pp. 362-368, 2004.

35. Charlier J. C., P.C. Eklund, J. Zhu and A.C. Ferrari, "Electron and Phonon Properties of Graphene: Their Relationship with Carbon Nanotubes", *Carbon Nanotubes*, Berlin/Heidelberg Springer-Verlag 2008.

36. Akturk A. and N. Goldsman, "Electron transport and full-band electron-phonon interactions in graphene", *Journal of Applied Physics*, Vol. 103, pp. 053702-05710, 2008.

37. Graf D., F. Molitor, K. Ensslin, C. Stampfer, A. Jungen, C. Hierold and L. Wirtz, "Spatially Resolved Raman Spectroscopy Of Single and Few-Layer Graphene", *Nano Letters*, Vol. 7, pp. 238-242, 2007.